United States
Department
of Agriculture

Forest Service

**Rocky Mountain
Research Station**

Research Paper
RMRS-RP-4 Revised

March 1998, revised
February 2004

FARSITE: Fire Area Simulator—Model Development and Evaluation

Mark A. Finney

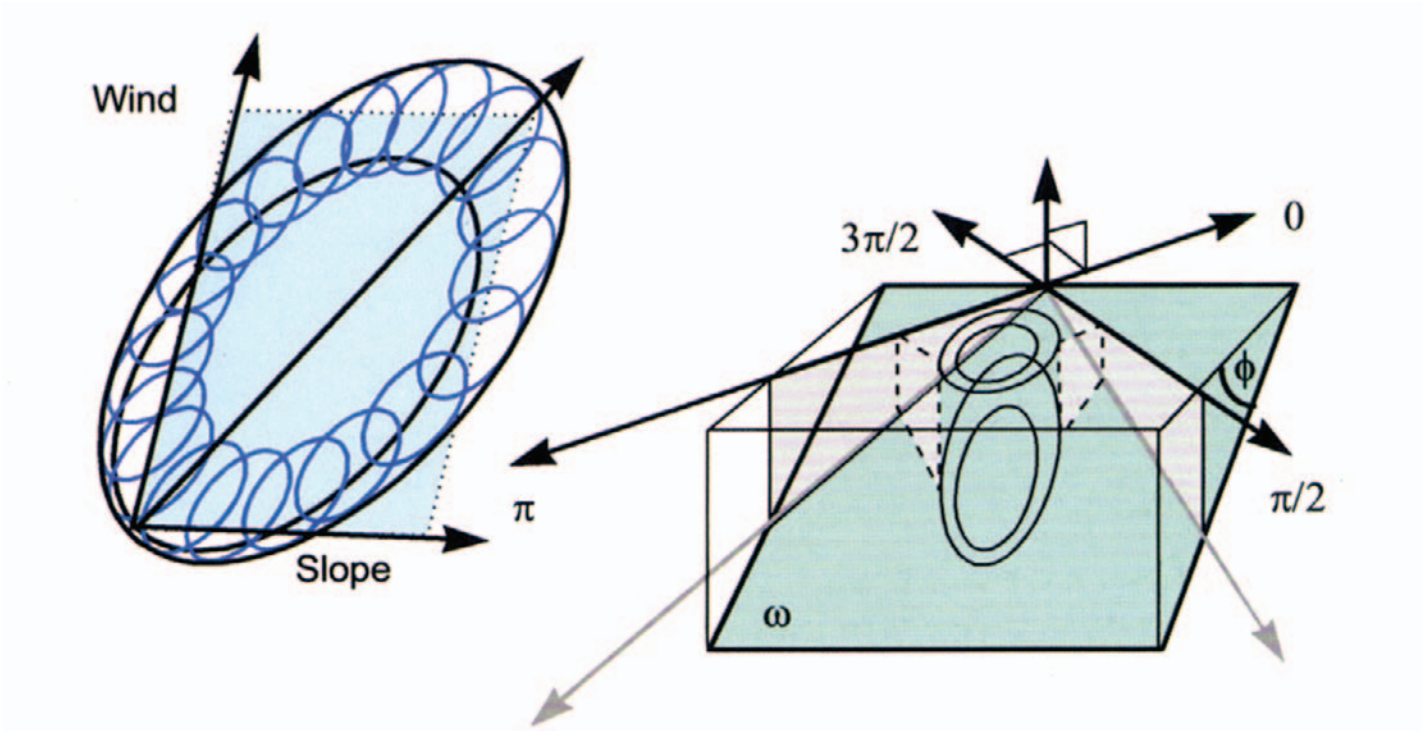

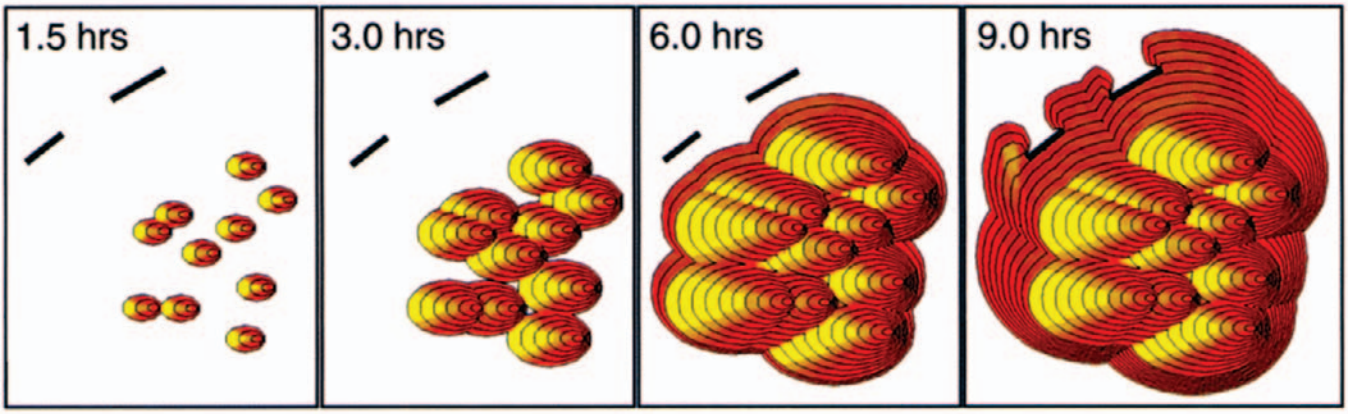

The Author

Mark A. Finney is a Research Scientist with Systems for Environmental Management in Missoula, MT. He has been doing research in cooperation with the Rocky Mountain Research Station (formerly the Intermountain Research Station at the Intermountain Fire Sciences Laboratory) in Missoula since 1993. Before that he spent two years as Researcher with Sequoia National Park. He holds a Ph.D. degree from the University of California, Berkeley, in wildland resource science (1991), an M.S. degree in forest science from University of Washington (1986), and a B.S. degree in forest management from Colorado State University (1984).

Research Summary

This paper reports on the structure of a fire growth simulation model, *FARSITE*, and its performance under simplified test conditions. *FARSITE* incorporates existing models of surface fire, crown fire, point-source fire acceleration, spotting, and fuel moisture. This documentation of how the simulation was constructed, and how the individual fire behavior models perform, will be useful to researchers and managers who use *FARSITE* or are interested in fire growth simulation. The models were integrated using a vector propagation technique for fire perimeter expansion that controls for both space and time resolution of fire growth over the landscape. The model produces vector fire perimeters (polygons) at specified time intervals. The vertices of these polygons contain information on the fire's spread rate and intensity, which are interpolated to produce raster maps of fire behavior. Because fire behavior at each vertex is assumed independent of the others, the simulation outputs illustrate the strict spatial consequences to fire behavior of incorporating the models into a two-dimensional simulation. Simplified test conditions show that surface fire growth and intensity conform to idealized patterns. Similarities also exist between simulated crown fires and observed patterns of extreme wind-driven fires. Complex patterns of fire growth and behavior result from the spatial and temporal dependencies in the model. The limitations and assumptions of this approach are discussed.

Acknowledgments

This document was prepared under cooperative agreement INT-95065-RJVA, between Systems for Environmental Management and the Fire Behavior Research Work Unit of the Rocky Mountain Research Station. Development, testing, documentation, and training of the *FARSITE* model was funded by the USDI National Park Service, National Interagency Fire Center, Boise, ID; the USDA Forest Service, Intermountain Fire Sciences Laboratory, Fire Behavior Research Work Unit, Missoula, MT (Cooperative Agreements INT-93854-RJVA and INT-95065-RJVA); and Forest Service Washington Office Fire and Aviation Management. The author thanks Marty Alexander, Pat Andrews, Judy Beck, Bob Keane, and Joe Scott for their reviews, comments, and suggestions.

Contents

Software Availability

FARSITE software and users guide are available free of charge electronically from:

http://www.farsite.org

and by mail from:

FARSITE
Intermountain Fire Sciences Laboratory
PO Box 8089
Missoula, MT 59807

FARSITE: Fire Area Simulator—Model Development and Evaluation

Mark A. Finney

Introduction: Two-Dimensional Models of Fire Growth

Researchers and land managers are increasingly interested in fire and ecosystems at larger spatial and temporal scales. They look to ecological models, particularly for fire, at landscape levels for use in management operations, planning, and scientific analyses. Until now, no models have attempted to integrate the many aspects of fire behavior that are already established individually. This paper reports on the structure of the two-dimensional deterministic fire growth model *FARSITE* (Fire Area Simulator, Finney 1994) and the output under simplified test conditions. The simulator incorporates existing fire behavior models of surface fire spread, crown fire spread, spotting, point-source fire acceleration, and fuel moisture. It demonstrates the linkages between existing fire behavior models and the consequences to spatial patterns of fire growth and behavior. This is particularly useful for exploring the connections between different fire behavior models, revealing the implications of their assumptions to fire growth, and identifying missing components among the various models.

Two-dimensional fire shapes are assumed to be generally ellipsoidal under uniform conditions. Uniform conditions occur when factors affecting fire behavior (fuels, weather, topography) are spatially and temporally constant, although these conditions rarely exist in nature. The most common model for fire shape is the simple ellipse (Van Wagner 1969). Its relatively straightforward mathematics allow computation of fire growth in perimeter or area as well as fire behavior (Catchpole and others 1982, 1992). Observations under relatively uniform field conditions have suggested fire shapes ranging from roughly egg shaped (Anderson 1983; Peet 1967) to fan shaped (Byram 1959). Some of these differences were likely caused by variation in environmental or spread conditions inherent to empirical fire data. However, Richards (1993) found that none of these shapes could be mathematically explained based on simple variability in windspeed or direction. Green and others (1983) concluded a simple ellipse fit observed fire growth data as well as other shapes. Regardless of the correct shape (if a single one exists), the eccentricity of the fire is known to increase with increasing windspeed or slope steepness or both (Alexander 1985). The change in shape has been assumed to be exponential and independent of the type of fuel in which the fire is burning (Anderson 1983), although data from grass fires suggests models of a different form could be applicable to those fuels (McArthur 1966).

Computerized models of fire growth have been a subject of research for several decades. Computational methods are used to automate the application of fire shape models to nonuniform conditions by assuming local uniformity (local to segments of the fire perimeter). The most common

approach has been to simulate fire growth as a discrete process of ignitions across a regularly spaced landscape grid (hereafter referred to as cellular models). The model by Kourtz and O'Regan (1971) computed the time for fire to travel between the eight neighboring cells or nodes on a rectangular grid. Successive calculations were performed for the individual cell that had the soonest arrival time. Geometric distortion to the fire shapes is produced by the fixed number of regular pathways for fire travel. Distortion is reduced by increasing the number of neighboring cells considered to be influenced by each cell in the fire spread calculations (Feunekes 1991; French 1992; Kourtz and others 1977; O'Regan and others 1976). Other cellular techniques also exist. Some use templates of varying shapes and sizes to represent the influence of a burning cell on its neighbors (Green 1983), or describe the transfer of fractional burned area between neighboring cells (Karafyllidis and Thanailakis 1997; Richards 1988). Others use stochastic percolation techniques (Beer and Enting 1990; Von Niessen and Blumen 1988) or fractal algorithms (Clarke and others 1994) to reflect uncertainty in spread though a regular landscape matrix. Some cellular techniques can be modified to reproduce the theoretical ellipsoid fire shapes with minimal distortion under uniform conditions (French 1992; Xu and Lathrop 1994). In general, cellular models have had diminishing success in reproducing the expected two-dimensional shapes and growth patterns as environmental conditions become more heterogeneous (French 1992). For example, cellular models have difficulty in responding appropriately to temporal changes such as shifting windspeed and direction as well as fuel moisture.

These problems with cellular models are avoided by the vector or wave approach to fire growth modeling (Huygens' principle). Here the fire front is propagated as a continuously expanding fire polygon at specified timesteps (Anderson and others 1982). It is essentially the inverse of the cellular method. The fire polygon is defined by a series of two-dimensional vertices (points with X,Y coordinates). The number of vertices increases as the fire grows over time (polygon expands). The expansion of the fire polygon is determined by computing the spread rate and direction from each vertex and multiplying by the duration of the timestep. Spread direction and rate normal to the fire front is determined from the direction and rate of maximum spread by an elliptical transformation (Richards 1995). The reliance on an assumed fire shape, in this case an ellipse, is necessary because the spread rate of only the heading portion of a fire is predicted by the present fire spread model (Rothermel 1972). Fire spread in all other directions is inferred from the forward spread rate using the mathematical properties of the ellipse. It is most common to assume that the ignition point or fire origin is coincident with the rear focus of the ellipse (Alexander 1985; Bratten 1978). Although not necessarily correct (Bilgili and Methven 1990; Catchpole and others 1982; Green and others 1983) this does provide an implicit backing fire spread rate (Alexander 1985). Alternatively, the location of the fire origin along the major axis of the ellipse could be computed from an independently calculated backing spread rate (for example, the constant no-wind-no-slope spread rate; see Rothermel 1983). These different methods, however, will probably be of little consequence to the practical application of a fire growth model until the greater uncertainties are resolved as to how wind, slope, and fuels affect fire shapes.

The concept of applying Huygens' principle to model fire growth simply involves using the fire environment at each vertex on the fire perimeter to

dimension and orient an elliptical wavelet at each timestep (fig. 1). Calculations at each vertex of the fire front are assumed independent of the others. The shape and direction of the ellipse are determined by wind-slope vector while the size is determined by the spread rate and the length of the timestep. The implementation of this in a practical fire growth model is more complex and is discussed in detail below.

Huygens' principle has been applied to fire growth modeling in various forms. The earliest application found for a vector model was the "radial fire propagation model" by Sanderlin and Sunderson (1975). It used gridded weather inputs and a rasterized landscape of fuels and topography to provide a reasonable approximation of observed fire growth (Sanderlin and Sunderson 1975; Sanderlin and Van Gelder 1977). The essential mathematics and many of the complications of the vector approach were first identified here. Anderson and others (1982) brought the terminology and concept of Huygens' principle to the fire literature. They described the mathematics and found the technique suitable as a fire growth model after comparing their simulation to data from a test fire. French and others (1990) and French (1992) employed a graphical technique that used computer graphics block-copy techniques to produce fire fronts. The "four-point" technique (Beer 1990; French 1992) used four points on an elliptical perimeter that correspond to its major and minor axes as the propagation points that form the new fire perimeters. Richards (1990) analytically derived a differential equation that propagates any point using an elliptical fire shape. Richards' (1990) technique is employed in the *FARSITE* model and uses the vertices of the fire perimeter polygon as the propagation points. The same result is achieved by the method of Roberts (1989; discussed by French 1992) in which the line segments between the vertices are the objects of propagation. Richards (1995) has simplified and extended his equations from Richards (1990) to

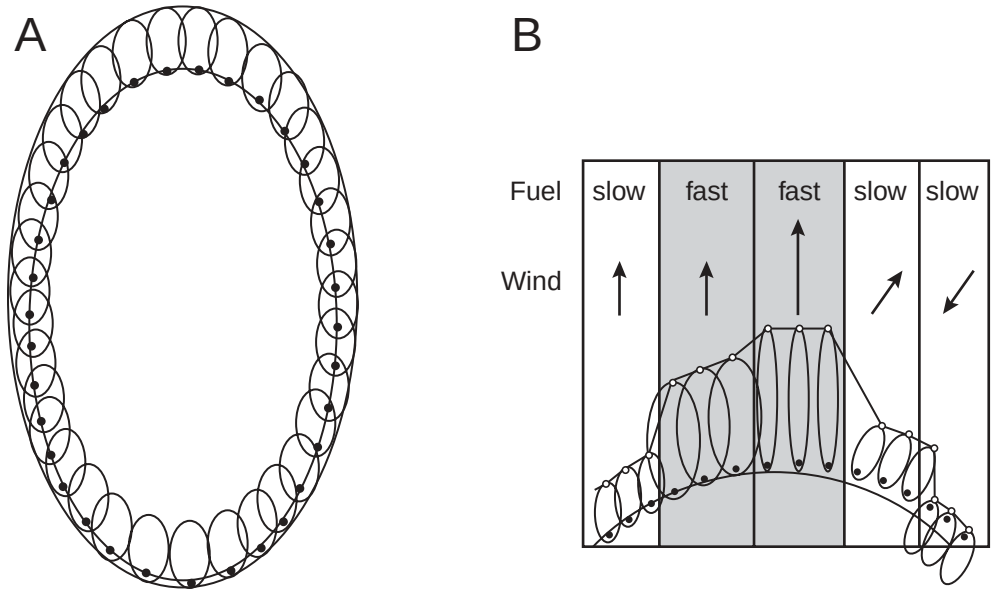

Figure 1—Illustration of Huygens' principle using elliptical wavelets. **(A)** Uniform conditions use wavelets of constant shape and size to maintain the elliptical fire shape over time. **(B)** Nonuniform conditions showing the dependency of wavelet size on the local fuel type but wavelet shape and orientation on the local wind-slope vector.

expand fire shapes other than the simple ellipse (for example, a lemniscate and double ellipse). Dorrer (1993), Knight and Coleman (1993), and Wallace (1993) have also developed procedures for computing fire perimeter positions based on Huygens' principle of wave propagation.

Fire Simulation Using Huygens' Principle

A number of computer applications have demonstrated the use of Huygens' principle for modeling surface fire growth (Coleman and Sullivan 1996; Finney 1994; Finney and Ryan 1995; Knight and Coleman 1993; Richards and Bryce 1995). This paper describes (1) the use of the Huygens' principle technique to include additional models for crown fire, spotting, acceleration, and fuel moisture, and (2) the spatial patterns of fire growth and intensity that result from the integration of these models under varying environmental conditions. The mathematical notation used was as close as possible to the original sources. Explanation of the symbols is found in appendix A.

The method chosen to implement Huygens' principle as a fire growth model was developed by Richards (1990, 1995). His differential equations describe the expansion of an elliptical wave front from a series of vertices that define the edge of a fire. Huygens' principle assumes that each vertex can serve as the source of an independent elliptical expansion. The information required at each vertex includes (1) the orientation of the vertex on the fire front in terms of component differentials (m) x_s, y_s, (2) the direction of maximum fire spread rate θ (the resultant wind-slope vector, radians azimuth), and (3) the shape of an elliptical fire determined from the conditions local to that vertex in terms of dimensions a, b, c (m min^{-1}; fig. 2). From these inputs, Richards' (1990) equation computes the orthogonal spread rate differentials (m min^{-1}) X_t and Y_t for a given vertex:

$$X_t = \frac{a^2 \cos\theta(x_s \sin\theta + y_s \cos\theta) - b^2 \sin\theta(x_s \cos\theta - y_s \sin\theta)}{(b^2(x_s \cos\theta + y_s \sin\theta)^2 - a^2(x_s \sin\theta - y_s \cos\theta)^2)^{1/2}} + c \sin\theta \quad [1]$$

$$Y_t = \frac{-a^2 \sin\theta(x_s \sin\theta + y_s \cos\theta) - b^2 \cos\theta(x_s \cos\theta - y_s \sin\theta)}{(b^2(x_s \cos\theta + y_s \sin\theta)^2 - a^2(x_s \sin\theta - y_s \cos\theta)^2)^{1/2}} + c \cos\theta \quad [2]$$

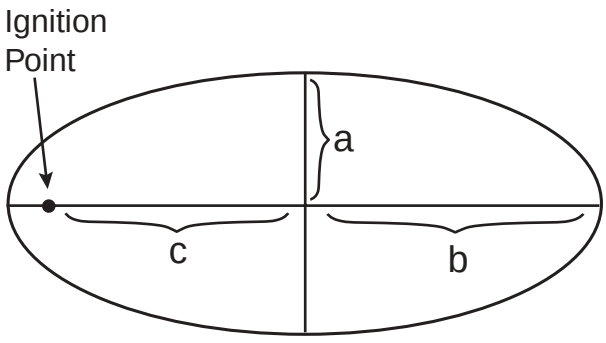

Figure 2—Dimensions of elliptical wavelets used in computing fire growth with equations [1] and [2] (after Richards 1990). Dimension *a* corresponds to ½ the minor axis (lateral from the center), *b* identifies ½ the major axis (forward from the center), and *c* is the distance forward of the ignition point to the center.

Transformations for Sloping Terrain

Richards' (1990, 1995) equations were originally developed for flat terrain. On flat terrain, a horizontal coordinate system remains unchanged when projected onto the ground surface. This is not the case for sloping terrain. It is crucial for all *inputs and outputs* associated with equations [1] and [2] to be referenced by coordinates of the surface plane local to each vertex (x_i, y_i). All vertices for all fire polygons are stored by the computer, however, in the common horizontal plane. This means that the inputs to equations [1] and [2] (x_s, y_s, and θ) must be transformed from the horizontal to the surface plane, and outputs (X_t, Y_t) must be transformed from the surface plane back to the horizontal plane.

The angle differentials x_s and y_s determine the direction normal to the fire front for each vertex (x_i, y_i) in a plane parallel to the ground surface. They are transformed from their original horizontal values by adding or subtracting a slope correction D_i (m) depending on the aspect ω_i (radians) of the i^{th} vertex:

$$x_s = (x_{i-1} - x_{i+1}) \pm D_i \sin\omega_i \quad [3]$$

$$y_s = (y_{i-1} - y_{i+1}) \pm D_i \cos\omega_i \quad [4]$$

where D_i is the difference between the distances measured for the perimeter segment (x_{i-1}, y_{i-1})–(x_{i+1}, y_{i+1}) on the horizontal and local sloping plane at the i^{th} vertex in the aspect direction:

$$D_i = \left[(x_{i-1} - x_{i+1})^2 + (y_{i-1} - y_{i+1})^2\right]^{1/2} \cos\delta_i(1 - \cos\phi_i) \quad [5]$$

ϕ_i is the local slope (radians) in the aspect direction ω_i (radians), δ_i is the difference between the aspect direction ω_i and the orientation angle of the perimeter segment as referenced on the coordinate system of the surface plane:

$$\delta_i = \tan^{-1}\left(\frac{\tan(\omega_i - \alpha_i)}{\cos\phi_i}\right) \quad [6]$$

where α_i is the orientation angle (radians) of the perimeter segment on the horizontal plane:

$$\alpha_i = \tan^{-1}\left[(y_{i-1} - y_{i+1})/(x_{i-1} - x_{i+1})\right] \quad [7]$$

These quantities are approximations to the normal angle on the fire front because the vertices used to compute D_i may lie in different planes in heterogeneous topography.

A similar but reverse procedure is used to transform the spread rate differentials (X_t and Y_t) to the horizontal plane (X_t' and Y_t'):

$$X_t' = X_t \pm D_r \sin\omega_i \quad [8]$$

$$Y_t' = Y_t \pm D_r \cos\omega_i \quad [9]$$

where D_r is the difference in spread rates (m min^{-1}) between the horizontal plane and the local sloping plane in the aspect direction:

$$D_r = \left[X_t^2 + Y_t^2\right]^{1/2} \cos(\omega_i - \tan^{-1}(Y_t / X_t))(1 - \cos\phi_i) \quad [10]$$

and is added or subtracted from the spread components depending on the aspect angle. Thus, the new horizontal coordinates for the i^{th} vertex are the products of the timestep and X_t and Y_t. The horizontal spread distance in that timestep is calculated with the Pythagorean theorem.

Vectoring Wind and Slope

The symbol θ in the equations [1] and [2] represents the angle of the resultant wind-slope vector for the direction of maximum fire spread ($0 \leq \theta \leq 2\pi$) on the local slope at a given vertex (x_i, y_i). This resultant vector was calculated for surface fires using the dimensionless coefficients for midflame windspeed Φ_w and slope Φ_s from the Rothermel fire spread equation (Rothermel 1972; Wilson 1980):

$$\Phi_s = 5.275\beta^{-0.3}\tan\phi^2 \quad [11]$$

$$\Phi_w = C(3.281U)^B\left(\frac{\beta}{\beta_{op}}\right)^{-E} \quad [12]$$

where β is the packing ratio of the fuel bed and ϕ is the slope (radians), U is the midflame windspeed (m s^{-1}), and the C, B, and E coefficients are functions of the fuel particle sizes in the fuel bed (Burgan 1987; Rothermel 1972).

The component vectors used for the spread direction of surface fires are highly dependent on characteristics of the surface fuel bed and thus not necessarily applicable to determining the spread direction of active crown fires. However, since the spread rate of active crown fires used in *FARSITE* was taken from the correlation with surface spread rate for fuel model 10 (Rothermel 1991, see the Crown Fire section later in this paper), the present formulation used the wind-slope vector for crown fire spread direction as calculated from these slope and wind coefficients (wind reduction factor of 0.4). In fact, this wind reduction factor is not much different from the "midflame" windspeed for crown fires assumed by Rothermel (1991) to be ½ the open wind (6.1 m above ground, see the next section on Elliptical Dimensions).

Note that vectoring the wind and slope requires the angle difference between each component to be expressed on the local surface plane. This is accomplished by substituting the horizontal wind azimuth (as obtained from input data) for the segment orientation angle α_i in equation [6]. The surface angle differs from the horizontal angle when aspect is not aligned with a cardinal direction.

Elliptical Dimensions

The dimensions a, b, c for equations [1] and [2] describe the shape of an elliptical fire produced at a given vertex. As Alexander (1985) states, it is typically assumed that the effects of wind and slope on fire shape are proportional to their effect on forward spread rate. This assumption, however, has not really been verified. Fire shapes have only been determined empirically and only with respect to measured windspeed. Shape may be affected differently by wind and slope because of different contributions of convective and radiative heat transfer to fire spread.

In the present model, however, the fire shape was computed at each vertex using the "effective" midflame windspeed (U m s^{-1}). It represents the *virtual* windspeed that by itself would produce the combined effect of slope and wind on fire spread rate. For surface fires, it is obtained from the resultant vector of midflame wind and slope (equations [11] and [12]) where equation [12] is rearranged to solve for U. The midflame wind for surface fires is reduced for stand height and canopy cover (Albini and Baughman 1979, see the section on Weather and Wind inputs, equation [43]). The "midflame" wind for active crown fire is assumed to be ½ the open wind at the reference height (6.1 m) (Rothermel 1991). A separate vectoring was required to obtain the elliptical dimensions of active crown fires. Without knowing how slope effects crown fire shape, the nonlinear effects of slope and wind on surface fire spread rate were ignored for vectoring crown fire midflame winds. This was justified given that the nonlinearity diminishes as winds increase (Rothermel 1972) and that active crown fire is typically observed with high winds. Thus, the vectoring uses the actual values for ½ open windspeed and the slope-equivalent windspeed for the surface fuel (obtained from equations [11] and [12]).

The dimensions of elliptical fires have been related to windspeed using a number of empirical formulas (Alexander 1985; Andrews 1986; Bilgili and Methven 1990; Forestry Canada Fire Danger Group 1992; Rothermel 1991). These formulas have different forms and produce various fire shapes for a given windspeed. Regardless of which one (if any) is most accurate, the range and uncertainty in windspeed over time and with vertical height, forest structure, and uneven terrain, accounts for at least as much variation in fire shape as any of the individual models. Thus, for the present formulation, the relationship developed by Anderson (1983) was chosen for the length to breadth ratio (LB) assuming the fires grow as a single ellipse (Alexander 1985) (not a double ellipse):

$$LB = 0.936\, e^{(0.2566U)} + 0.461\, e^{(-0.1548U)} - 0.397 \quad [13]$$

Anderson's (1983) original equation was modified by subtracting a constant 0.397 from LB. This was needed to have $LB = 1.0$ on flat terrain with no wind. It may, in fact, benefit the accuracy of fire growth predictions because the natural variation in wind direction at high frequencies (relative to the data used for input as U) effectively decreases LB for real fires (Richards 1993; Simard and Young 1978). Also, Anderson's (1983) equation can produce very eccentric fires with high winds (Rothermel 1991). Ellipses with LB greater than 8 are truncated to that dimension based on the maximum of empirical data referenced by Alexander (1985). This does not necessarily constrain crown fires from achieving more eccentric shapes; spotting ahead of the main fire front often increases the effective eccentricity of the overall fire pattern.

Assuming the rear focus of the ellipse to be the fire origin (Alexander 1985), the head to back ratio is described as:

$$HB = \left(LB + (LB^2 - 1)^{0.5}\right) / \left(LB - (LB^2 - 1)^{0.5}\right) \quad [14]$$

from which the a, b, and c dimensions of the elliptical axes (used in equations [1] and [2]) can then be computed in units of fire spread rate R (m min^{-1}) from either surface or crown fire:

$$a = 0.5(R + R/HB)/(LB) \quad [15]$$

$$b = (R + R/HB)/2.0 \quad [16]$$

$$c = b - R/HB \quad [17]$$

Fire Behavior Models

The fire behavior models currently used by wildland fire managers are specific to distinct "types" of fire behavior. Separate models are used for surface fire, crown fire, spotting, and point-source fire acceleration. These behaviors are really abstractions of an overall three-dimensional process of unconfined combustion that links implicitly to the environment through heat and mass transfer feedbacks. Models of this form (for example, Clark and others 1996a,b; Linn 1997) have not yet been developed to the point of practical application. In the present simulation, the separate fire models are linked explicitly in the two-dimensional simulation technique and are not coupled to the environmental inputs.

The existing models of fire behavior are all formulated as one-dimensional point calculations. They produce spread rates or distances from conditions specified at a particular geographic point. This formulation fits conveniently into the Huygens' principle approach for wave-front modeling because both the wave front and the source of fire calculations are discrete vertices with two-dimensional coordinates. Thus, the one-dimensional calculations are extended to two-dimensions by virtue of being assigned to vertices that define a two-dimensional fire front. The fire front is represented by a series of vertices from which data on the fire environment are obtained. At each vertex, the environmental variables (fuels, weather, topography) are used to compute fire behavior. An assumed fire shape (ellipse) is parameterized at each vertex (equations [13] through [17]) from the effective midflame windspeed at that point (equations [11] and [12]). Using the orientation of each vertex on the fire front (equations [3] through [7]) and the effective wind direction (equations [11] and [12]), the fire spread rate and direction are computed (equations [1] and [2]) and transformed to the horizontal (equations [8] through [10]). Multiplying by a constant timestep produces the fire position at the end of that period.

The linkage among the existing fire behavior models relies on an assumed sequence of fire activity. First, a fire may spread as a surface fire. It burns in the grass, shrubs, or downed woody fuels in contact with the ground surface. If the environmental conditions permit, the fire will accelerate toward some new equilibrium spread condition. Given sufficient fuels, weather, and topography, the fire may make the transition to burning in the aerial fuels of tree crowns (crown fire). If crown fuels are ignited, trees are assumed to torch and can loft embers. The following models were used in *FARSITE* to represent these phases of fire activity.

Surface Fire

The surface fire spread model used in *FARSITE* was the Rothermel spread equation (Albini 1976; Rothermel 1972). It computes the steady-state fire spread rate (m min^{-1}) in a plane parallel with the ground surface at every vertex:

$$R = \frac{I_R \xi \left(1 + \Phi_w + \Phi_s\right)}{\rho_b \varepsilon Q_{ig}} \qquad [18]$$

where:

R = heading fire steady state spread rate (m min^{-1})
I_R = reaction intensity (kJ min^{-1} m^{-2})
ξ = the propagating flux ratio
ρ_b = ovendry bulk density, kg m^{-3}
ε = effective heating number, dimensionless
Q_{ig} = heat of pre-ignition, kJ kg^{-1}

Wind and slope coefficients (equations [11] and [12]) are accounted for by the additive terms Φ_w and Φ_s, respectively. Fuel bed characteristics are specified according to the format of fire behavior fuel models used in BEHAVE (Albini 1976; Anderson 1982; Andrews 1986; Burgan and Rothermel 1984). Fireline intensity I_b (Byram 1959) describes the rate of energy release per unit length of the fire front (kW m^{-1}):

$$I_b = hwR/60 \quad [19]$$

where h represents the heat yield of the fuel (kJ kg^{-1}, total heat less the energy required for vaporizing moisture), w the weight of the fuel per unit area (kg m^{-2}) burned in the flaming front, and $R/60$ is fire spread rate converted to units of (m s^{-1}). It is calculated in BEHAVE and *FARSITE* as (in SI units from Wilson 1980):

$$I_b = \frac{I_R}{60}\frac{12.6R}{\sigma} \quad [20]$$

where σ is the characteristic surface area to volume ratio of the fuel bed (m^{-1}). The frontal fire characteristics (spread rate, fireline intensity, and so forth) calculated for a steady-state fire are dependent on the current environmental conditions such as fuel characteristics and moisture, windspeed and direction, and topographic slope and aspect. All of these parameters must be available or computable at any point on the landscape at any time.

Crown Fire

Crown fire is the combustion of tree crowns that overlie the surface fire and surface fuels. The crown fire model used in *FARSITE* was developed by Van Wagner (1977, 1993) and is similar to its implementation in the Canadian Forest Fire Behavior Prediction System (Forestry Canada Fire Danger Group 1992). It determines if the fire remains burning in the surface fuels or makes a transition to burning in crown fuels, and whether it spreads actively through the tree crowns or simply torches individual trees. The model assumes that the threshold for transition to crown fire I_o (kW m^{-1}) is dependent on the crown foliar moisture content M (percent on dry weight basis: determines crown ignition energy) and the height to crown base *CBH* (m) (Van Wagner 1989):

$$I_o = (0.010\ CBH\ (460 + 25.9M))^{3/2} \quad [21]$$

Crown base height is the vertical distance between the ground surface and the base of the live crown fuels, but in practice should incorporate the presence or effect of "ladder" fuels (Alexander 1988; Forestry Canada Fire Danger Group 1992; Van Wagner 1993). That is, dead branches or small trees connecting the surface fire to the crown fuels that would effectively lower the

nominal value of *CBH*. Transition to some form of crown fire occurs at the *ith* vertex if the surface fire intensity, calculated by equation [20] meets or exceeds I_o. The "type" of crown fire depends on the threshold for active crown fire spread rate *RAC* (Alexander 1988):

$$RAC = 3.0 / CBD \quad [22]$$

where *CBD* is the crown bulk density (kg m^{-3}) and 3.0 is the product of an empirical constant defining the critical mass flow rate through the crown layer for continuous flame (0.05 kg m^{-2} s^{-1}) and a conversion factor (60 s min^{-1}). Van Wagner (1977) identifies three types of crown fire determined by the I_o and *RAC*:

1. Passive Crown Fire ($I_b >= I_o$ but $R_{Cactual} < RAC$),
2. Active Crown Fire ($I_b >= I_o$, $R_{Cactual} >= RAC$, $E < E_o$)
3. Independent Crown Fire ($I_b > I_o$, $R_{Cactual} >= RAC$, $E > E_o$)

where E and E_o represent the actual and critical energy flux, respectively in the advancing direction. Van Wagner (1993) suggests independent crown fires are very rare and short lived. Thus, neither E nor E_o are calculated, and independent crown fire is not incorporated in this analysis or in *FARSITE*.

The spread rate of a passive crown fire is assumed equal to that of the surface fire. The actual active crown fire spread rate at the *ith* vertex $R_{Cactual}$ (m min^{-1}) is determined from the maximum crown fire spread rate (R_{Cmax}) as:

$$R_{Cactual} = R + CFB(R_{Cmax} - R) \quad [23]$$

if $R_{Cactual}$ meets or exceeds *RAC,* where:

$$R_{Cmax} = 3.34 R_{10} E_i \quad [24]$$

and $3.34R_{10}$ is the active crown fire spread rate (m min^{-1}) determined from a correlation with the forward surface fire spread rate for U.S. fuel model 10 using a 0.4 wind reduction factor (Rothermel 1991). Although intended to represent the average crown fire spread rate (Rothermel 1991), the coefficient *3.34* was used here to determine the maximum crown fire spread rate. This implementation sought to minimize the possibility that spotting could be accounted for twice, first from its contribution to spread rates implicit in the data on which Rothermel's (1991) regression was based, and second from torching trees as modeled separately in this simulation (see below). Coefficients larger or smaller than 3.34 could also be justified given the variation observed in the regression (up to 1.7 times the mean) (Rothermel 1991). Nevertheless, this correlation remains independent of crown structure, and the uncertainties in predicting crown fire spread rates are not likely resolved through simple adjustment of the coefficient.

The quantity E_i is the fraction of the forward crown fire spread rate ($E_i \leq 1.0$) achievable at the *ith* perimeter vertex, given the orientation of that vertex relative to the maximum spread direction and the elliptical dimensions of the crown fire (see the earlier section on Elliptical Dimensions). *CFB* is the crown fraction burned, defined as the proportion of trees involved in the crowning phase of the fire (Forestry Canada Fire Danger Group 1992; Van Wagner 1993):

$$CFB = 1 - e^{-a_c(R - R_o)} \quad [25]$$

which depends on the exponent a_c that scales *CFB* to equal 0.9 when the surface fire spread rate reaches 90 percent of the difference between *RAC* and the critical surface fire spread rate R_o associated with the critical intensity for initiating crown fire (equation [21]):

$$a_c = \frac{-\ln(0.1)}{0.9(RAC - R_o)} \quad [26]$$

$$R_o = I_o \frac{R}{I_b} \quad [27]$$

Here R_o is computed from I_o using only the fraction of surface fuels consumed in the flaming front compared to total fuel consumption used by the Canadian Forest Fire Behavior Prediction System (Forestry Canada Fire Danger Group 1992; Van Wagner 1993).

Linking the Van Wagner (1977, 1993) crown fire model and the Rothermel (1972) fire spread equation required some additional decisions concerning active crown fire. The coefficient used to scale *CFB* in equation [25] is computed as described by Van Wagner (1993). The concept of a rapid transition from a passive to an active crown fire state was retained from Van Wagner (1977) and causes a discrete jump in fire spread rate when $R_{Cactual}$ meets or exceeds *RAC*. This differs from Van Wagner (1993) where spread rates for passive crown fires would smoothly increase as a function of *CFB*. A smooth increase in spread rate from a surface fire to an active crown fire could not be justified if crown fuels were not continuous for a given *CBD* or if the mechanism of the proposed gradual increase in fire spread rate was implicitly including short range spotting (accounted for separately in *FARSITE*). In a spatial context, the gradual increase also implies that passive crown fires in the backing directions could increase their spread rates against the wind or down slope by increasing *CFB*.

The intensity of a crown fire I_c (kW m^{-1}) is calculated for a given vertex by modifying equation [19] to include the combined loading of crown fuel and surface fuel consumed in the flaming front along with the fire spread rate for active crown fires ($R_{Cactual}$) or for passive crown fires (for example, the surface fire spread rate R):

$$I_c = 300\ (I_b / 300R + CFB \cdot CBD(H\text{-}CBH))\ R_{Cactual} \text{ or } R \quad [28]$$

where H is crown height (m) and the heat content of both surface and crown fuels is assumed to be 18000 kJ kg^{-1}.

Fire Acceleration

Fire acceleration is defined as the rate of increase in spread rate for a given ignition source assuming all fire environmental conditions remain constant. Other definitions of fire acceleration have included rate increases that arise because fire ignites additional fuels, fuels dry out during the day, or because windspeed increases (Cheney 1981; Cheney and Gould 1997). In a strict sense, fire spread rate increases in these situations because the environmental conditions are changing to create higher potential levels of a fire spread rate equilibrium. These kinds of changes are addressed as the simulation progresses through dynamic environmental conditions, not as acceleration.

Fire acceleration was incorporated into the *FARSITE* calculations to eliminate instantaneous jumps to faster spread rates that would follow

sudden increases in windspeed, steeper slopes, or changes to faster fuel types. The simple logarithmic formula for point-source fires of the Canadian Forest Fire Behavior Prediction System assumes the fire spread rate R_t at time t is dependent on only the time allowed for accelerating to the maximum rate possible under the current conditions (Forestry Canada Fire Danger Group 1992; McAlpine and Wakimoto 1991):

$$R_t = R(1 - e^{-a_a t}) \quad [29]$$

where R is the equilibrium spread rate (m min^{-1}), t is the elapsed time (min), and a_a is a constant that determines the rate of acceleration. Acceleration rates are assumed to be independent of fire behavior. Values for a_a are adjustable by fuel type but have been suggested at 0.115 for point source fires in Canadian timber fuels to achieve 90 percent of the equilibrium fire spread rate in 20 minutes (Forestry Canada Fire Danger Group 1992). Line source fires are known to accelerate faster (Cheney and Gould 1997; Johansen 1987), having a_a set to 0.300 will give a time to 90 percent equilibrium of under 8 minutes. Crown fire acceleration rates are determined from a formula similar to that from the Canadian Forest Fire Prediction System (Forestry Canada Fire Danger Group 1992):

$$a_a = a_a - 18.8 CFB^{2.5} e^{(-8\ CFB)} \quad [30]$$

This allows for different acceleration coefficients a_a depending on fuel type and a line or point source fire. Equation [29] can be integrated to solve for the spread distance D after a given amount of elapsed time t (Forestry Canada Fire Danger Group 1992):

$$D = R\left(t + \frac{e^{-at}}{a_a} - \frac{1}{a_a} \right) \quad [31]$$

To control time and space resolutions during the simulation (described below), it becomes necessary to calculate the time for the fire to spread a given distance from its current spread rate, provided a new equilibrium spread rate. This is computed for each vertex by iterating equations [29] and [31] (Newton's method). With each iteration, the time t is reduced by the ratio of $(D\text{-}D_t)/R$ until $D\text{-}D_t$ is within some tolerance limit (10^{-6}). D_t is the spread distance required to achieve the current spread rate under current conditions plus the desired spread distance in the next timestep D_{t+1}:

$$D_t = R\left(T_t + \frac{e^{-a_a T_t}}{a_a} - \frac{1}{a_a} \right) + D_{t+1} \quad [32]$$

and T_t is the time required to achieve the current spread rate under current conditions:

$$T_t = ln(1\text{-}R_t/R)/a_a \quad [33]$$

Fires are assumed to decelerate instantly when encountering new environmental conditions that produce a slower fire spread rate.

Spotting

Spotting refers to new ignitions ahead of the main fire front started by firebrands lofted by the fire and transported by the wind. Spotting can

advance fire over barriers many kilometers away from the current fire perimeter and dramatically alter fire growth patterns and behavior. There have been few studies on ember production that would help determine ember quantities or size distributions generated by different fire or vegetation types (Muraszew and Fedele 1976). The simulation of spotting is thus restricted to determining the contact locations of standard firebrands of different sizes that are transported over heterogeneous topography. The model used here was based on Albini's (1979) equations for spotting from torching trees. Torching trees are a consistent source of embers that start spot fires because they produce many brands and are capable of lofting them high into the ambient winds.

The spotting distance in uneven terrain depends on ember size, the vertical windspeed profile, and the surface topography in the direction of ember travel. For a given ember shape and density, larger embers can burn longer but won't be lofted as high as small ones. Larger embers also achieve a higher terminal velocity and thus drop more quickly though the wind field. Albini's (1979) model calculates the height to which a particle is lofted as the height where the duration of the buoyant flow structure of the torching tree (t_f) equals the time required for the particle to travel upward from its source (t_t):

$$t_f = t_o + 1.2 + \frac{a_x}{3}\left(\left(\frac{b_x + z/z_F}{a_x}\right)^{3/2} - 1\right) \quad [34]$$

where:

z = particle height (m)
z_F = flame height (m)

the constants a and b relate to the flame structure (Albini 1979):

$a_x = 5.963$
$b_x = 4.563$

and

$$t_t = t_o + t_1 + t_2 + t_3 \quad [35]$$

t_o is the time of steady burning of tree crowns. Both z_F and t_o are determined for characteristics of individual species, tree diameters, and numbers of torching trees in a group (Albini 1979).

t_1 is the time for a particle to travel from its initial height to the flame tip:

$$t_1 = 1 - \left(z_o/z_F\right)^{1/2} + \frac{v_o}{w_F}\ln\left(\frac{1 - v_o/w_F}{\left(z_o/z_F\right)^{1/2} - v_o/w_F}\right) \quad [36]$$

t_2 is the time for the particle to travel through the transition zone between the flame tip and the buoyant plume:

$$t_2 = 0.2 + B\left(\frac{D_p}{z_F}\right)^{1/2}\left(1 + B\left(\frac{D_p}{z_F}\right)^{1/2}\ln\left(1 + 1\Big/\left(1 - \left(\frac{D_p}{z_F}\right)^{1/2}\right)\right)\right) \quad [37]$$

and t_3 is the time for the particle to travel in the buoyant plume:

$$t_3 = \frac{a_x}{0.8 v_o / w_F}\left(\ln\left(\frac{1-0.8 v_o / w_F}{1-0.8 r\, v_o / w_F}\right) - 0.8\left(v_o \diagup w_F\right)(r-1) - \frac{1}{2}\left(0.8 v_o / w_F\right)^2 (r-1)^2\right) \quad [38]$$

where:

v_o = terminal velocity of the particle (m s^{-1})
w_F = flame gas velocity (m s^{-1})
r = $((b+z/z_F)/a)^{1/2}$
D_p = particle diameter (m)
B = 40
v_o/w_F = $B(D/z_F)^{1/2}$ (dimensionless)

Several assumptions are used for computing the lofting height of particles of a given diameter:

1. Particles are assumed to originate at the top of the canopy.
2. The base of the flame is assumed equal to half the stand height.
3. Particles are cylinders with constant specific gravity (0.3 g cm^{-3}) and drag coefficient C_D (1.2).
4. Particles are lofted vertically above the burning tree (for example, no downwind travel occurs during lofting).

Once lofted, particles begin descending through the wind field. Windspeeds are assumed to have only a horizontal component and increase logarithmically from the reference velocity provided as a simulation input at a height of 6.1 m (20 ft) above the top of the vegetation. The particle descends at a decreasing rate because it loses density and volume during burning. This is reflected in its terminal velocity such that its elevation z at time t is:

$$z(t) = z(0) - v_o(0)\left(t/\tau - \frac{1}{2}(t/\tau)^2\right) \quad [39]$$

where

$$\tau = 4 C_D v_o(0) / K\pi g \quad [40]$$

K = 0.0064
g = acceleration of gravity (9.8 m s^{-2})

and its terminal velocity (m s^{-1}) is:

$$v_o = \left(\pi g \rho_s D_p / 2 C_D \rho_a\right)^{1/2} \quad [41]$$

ρ_s = density of charred wood cylinder (0.3 g cm^{-3})
ρ_a = density of air (1.2 X 10^{-3} g cm^{-3})
C_D = drag coefficient of cylindrical particle (1.2)

As the particle descends, its rate of travel in the horizontal direction (X) is determined by the windspeed at that height that decreases logarithmically toward the top of the canopy (H, m):

$$\frac{dX}{dt} = U_H \ln(z/z_o) / \ln(H/z_o) \quad [42]$$

where

z_o = the friction length (0.4306 H, m)
H = height (m) of the forest canopy

and the windspeed (m s^{-1}) at height H from Albini and Baughman (1979):

$$U_H = \frac{U_{20+H}}{\ln\left(\left(20+1.18H\right)/0.43H\right)} \quad [43]$$

Upon contact with the ground surface, a burning ember may ignite a new fire if:

1. It doesn't fall within a burned area.
2. It lands on a combustible substrate.
3. The fuel substrate is ignitable by the brand.

Brands still burning when reaching the ground can ignite new fires if they fall outside an existing fire polygon or inside a fire enclave (island of unburned fuel). The number of brands is then reduced by a simple percentage selected by the user to account for items 2 and 3 above. This "ignition frequency" attempts to represent the profusion of factors that affect ignition but that are not well quantified mechanistically or spatially. Important on this list is the fine scale heterogeneity of the fuel substrate. Fuels are assumed to be homogeneous at the scale of fire behavior models, but the small size of each ember makes a successful ignition sensitive to variations in fuel continuity at a similarly fine scale (for example, between individual elements of the fuel bed). Other factors known to affect ignition frequency include filtering by the forest canopy, the surface fuel moisture content, fuel temperature (Blackmarr 1972; Bradshaw and others 1984; Bunting and Wright 1974), and differing physical and thermal fuel properties (such as rotten wood or cattle dung) that vary spatially (Bunting and Wright 1974).

Ember particles obviously come in all shapes, sizes, and textures that affect the particle drag coefficient. The use of cylindrical brands has been justified given that differing drag coefficients would probably result in little net change in spotting distance over flat terrain (Albini 1979). Particles with higher drag would increase their downwind drift distance because of lower terminal velocity but also decrease their initial lofting height.

Simulation Function

Spatial Data Inputs

All fire growth simulations require spatial data that comprise the fuels, weather, and topographic elements of fire behavior. In this simulation, weather and winds are input as streams of data (see next section), whereas fuels and topography are provided as GIS raster themes (table 1, color plate 1). GIS data are provided in raster format to facilitate rapid access by the model to the necessary spatial data. Vector data could also be used (Coleman and Sullivan 1996) but would require access to information within each polygon for a given vertex. Raster resolutions of 25 to 50 m are most commonly available for topographic and satellite data and seem to provide an acceptable level of detail for heterogeneous landscapes.

Table 1—Raster inputs to *FARSITE* and their usage in the simulation.

Raster theme	Units	Usage
Elevation	m, ft	Used for adiabatic adjustment of temperature and humidity from the reference elevation input with the weather stream.
Slope	percent, °	Used for computing direct effects on fire spread, and along with Aspect, for determining the angle of incident solar radiation (along with latitude, date, and time of day) and transforming spread rates and directions from the surface to horizontal coordinates.
Aspect	° Az	See Slope.
Fuel model		Provides the physical description of the surface fuel complex that is used to determine surface fire behavior (see Anderson 1982). Included here are loadings (weight) by size class and dead or live categories, ratios of surface area to volume, and bulk depth.
Canopy cover	percent	Used to determine an average shading of the surface fuels (Rothermel and others 1986) that affects fuel moisture calculations. It also helps determine the wind reduction factor that decreases windspeed from the reference velocity of the input stream (6.1 m above the vegetation) to a level that affects the surface fire (Albini and Baughman 1979).
Crown height	m, ft	Affects the relative positioning of a logarithmic wind profile that is extended above the terrain. Along with canopy cover, this influences the wind reduction factor (Albini and Baughman 1979), the starting position of embers lofted by torching trees, and the trajectory of embers descending through the wind profile (Albini 1979).
Crown base height	m, ft	Used along with the surface fire intensity and foliar moisture content to determine the threshold for transition to crown fire (Alexander 1988; Van Wagner 1977).
Crown bulk density	kg m^{-3} lb ft^{-3}	Used to determine the threshold for achieving active crown fire (Van Wagner 1977, 1993).

Weather and Wind Inputs

Ideally, weather and wind data could be input to a fire growth simulation as three-dimensional grids for all variables involved in fire behavior and fuel moisture calculations. Indeed, fire growth simulations using Huygens' principle are not limited to the types or resolutions of weather and wind inputs. However, for practical applications (such as field-level fire growth projections), the weather and wind data must be extrapolated from a few weather recording stations that are representative of the fire location. The following two data streams were devised to provide the minimum set of inputs required to compute fuel moisture and fire behavior.

The weather stream consists of daily observations of minimum and maximum temperature and humidity, and of precipitation at a specified elevation (table 2). These data are used to generalize a diurnal weather pattern for a designated portion of the landscape so that dead woody fuel moistures can be calculated (see Fuel Moisture section). Temperature and humidity are assumed to respond inversely over time as approximated by a cosine curve between the maxima and minima (fig. 3) (Beck and Trevitt 1989; Rothermel and others 1986). Adiabatic adjustment from the input elevations to any point on the landscape determines the local temperature (1 °C per 100 m) and humidity (0.2 °C per 100 m). Precipitation is assumed spatially constant across the designated portion of the landscape. These lapse rates assume a well mixed atmosphere without inversions (Rothermel and others 1986).

Table 2—Formatted input stream for weather variables used in *FARSITE* simulation.

Month	Day	PPT	Hour		Temperature		RH		Elevation
			AM	PM	Min	Max	Max	Min	
		*in*100*			----- °F ----		--- *percent* --		- *ft* -
08	29	00	0600	1500	45	78	65	28	5600
08	30	00	0600	1500	46	78	62	29	5600
08	31	00	0600	1500	50	82	54	25	5600
09	01	10	0600	1500	51	80	57	24	5600
09	02	00	0600	1500	49	75	56	30	5600

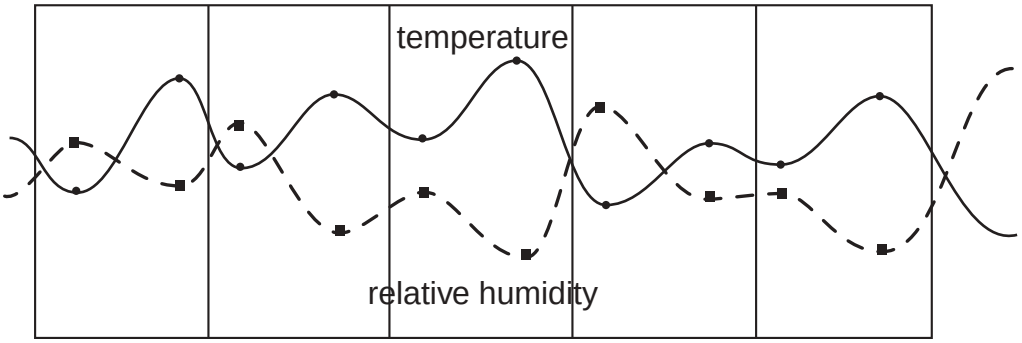

Figure 3—Modeled diurnal pattern of temperature and humidity variation for 5 days. Cosine interpolation is used to generalize the diurnal pattern given maxima and minima (dots) for temperature and humidity at specific times in the weather stream (table 2).

The wind stream allows for event-driven changes in windspeed and horizontal direction as well as cloud cover (table 3). As with the weather stream, the wind and cloud data are assumed to apply uniformly to the designated area on the landscape. Wind inputs are required to reflect "open" conditions at 6.1 m (20 ft) above the top of the vegetation layer (trees, shrubs, and so forth). Windspeed is assumed everywhere to be parallel to the terrain. Wind reduction to the "midflame" height (*U;* Albini and Baughman 1979) assumes flat terrain and does not account for different wind exposures to surface fires that result for combinations of wind direction and topographic position (such as ridgetop versus sideslope versus valley bottom) (Albini and

Table 3—Formatted input stream for wind and cloud variables used in *FARSITE* simulation.

Month	Day	Hour, minute	Open windspeed	Wind direction	Cloud cover
			mph	°*Az*	*percent*
08	29	0000	0	65	0
08	29	0200	2	68	0
08	29	0230	3	56	0
08	29	0300	1	60	0
08	29	0500	8	65	0
08	29	0800	9	187	0
08	29	1132	7	211	0
08	29	1400	14	224	20
08	29	1800	11	220	40

Baughman 1979; Andrews 1986). For nonforested areas midflame windspeed is reduced to a nominal height equal to twice the fuel bed depth (Albini and Baughman 1979). For forested terrain the open windspeed is reduced locally by the canopy cover data provided as a spatial theme from the GIS:

$$U = \frac{0.555 U_{20+H}}{\sqrt{f 3.28H}\,\ln\left(\left.(20+1.18H)\right/ 0.43H\right)} \quad [44]$$

where:

H = height (m) of the forest canopy (from spatial inputs)
U_{20+H} = windspeed (m s^{-1}) at 6.1 m above the tree tops (20 ft)

$$f = \text{the crown filling fraction} = \frac{C}{100}\frac{\pi}{12} \quad [45]$$

and:

C = canopy cover from spatial inputs (percent, horizontal coverage)

Crown filling fraction is the fraction of crown space occupied by tree crowns (Albini and Baughman 1979). This fraction is related linearly to canopy cover in single story stands if tree crown volumes are constant for a given horizontal projection. Equation [45] assumes tree crowns are conical, occupying one-third the volume of a cylinder of the same dimensions. Multiplying by (π/4) accounts for gaps in a square horizontal packing of circular crowns. The calculated filling fraction reaches a maximum of about 0.26 that aligns with high estimates of f for dense mature stands (Albini and Baughman 1979). Canopy cover from 20 to 40 percent gives f–values of 0.05 to 0.10 that agree with the range for open stands reported by Albini and Baughman (1979). Variation would undoubtedly occur with stands of mixed species, multiple strata, different crown shapes, and tree arrangement. However, given the burden of additional input requirements, further refinement could not be justified without models of spatially dynamic wind fields that reflect the influence of topography, vegetation roughness, and neighboring vegetation structure.

Fuel Moisture

Dead woody fuel moisture varies over time as a function of fuel particle size, weather conditions, and exposure to wind and sun. The user provides an initial suite of fuel moistures (dead and live categories) by fuel model. Spatial variation in initial dead or live fuel moisture (because of elevation or aspect) can be approximated by (1) assigning custom fuel models (and associated initial conditions) to those areas, and (2) "conditioning" the dead fuels for a period before the fire simulation starts. The latter involves inserting some time (days or weeks) ahead of the actual simulation to force additional calculations of fuel moisture to precede the start of the fire simulation.

Throughout the simulation, *FARSITE* calculates the moisture contents (percent dry weight) of dead fuels in the time-lag categories required for the fire behavior models. As simulation time elapses, the influence of initial fuel moisture conditions diminishes (especially for fine fuels). The moisture model presently contained in the BEHAVE system (Hartford and Rothermel 1991; Rothermel and others 1986) is used to calculated 1 hr and 10 hr dead moisture contents. Equations from the National Fire Danger Rating System

(NFDRS) (Bradshaw and others 1984) are used to calculate 100 hr dead moisture. The fuel moistures on the landscape at each vertex of the fire polygon are computed at each timestep starting from initial conditions. This procedure has proven faster than computing fuel moistures exhaustively for all portions of a landscape at all timesteps because fuel moistures are only required for the vertices involved in fire growth during the current timestep. Live fuel moistures (woody and herbaceous) are assumed constant during the simulation unless manually changed.

Dead fuel moisture is well known to depend on heating and drying by direct solar radiation. The above models incorporate effects of solar energy received during daytime hours on fuel moisture calculations. Sunlight is attenuated by the geometry of sun angle and terrain for a given latitude, date, and time of day (Rothermel and others 1986). Solar irradiance may then be reduced by cloud cover (input from the wind stream above) and forest canopy cover (input from GIS data).

Control of Spatial and Temporal Resolution

The simulation process (table 4) shows the nested logic of the model structure. The total length of the simulation is broken down into timesteps. In each timestep, the growth of each fire polygon is computed as the aggregation of spread from its vertices. Separate fires are merged after each timestep is completed.

Three simulation parameters are used to control the spatial and temporal resolution of the calculations: (1) the maximum timestep, (2) the distance resolution, and (3) the perimeter resolution. Vector models of fire growth use a *timestep* along with the spread rate of the fire to compute the distance traveled by fire at the vertices of the fire edge. In a practical sense, the timestep is the maximum amount of time that environmental conditions are assumed constant so that fire growth can be projected. The *FARSITE* model dynamically adjusts the timestep to achieve a specified level of spatial detail determined by the *distance resolution*. The timestep may also be reduced to ensure the use of all the time-specific wind data if the time until the next wind observation is less than that required to achieve the distance resolution. The distance resolution is the maximum horizontal spread distance allowed before new information from the landscape is required. It is the resolution in the radial spread direction. The *perimeter resolution* is the maximum distance allowed between vertices of the fire polygon; convex portions of the fire perimeter are expanding and the vertices become separated over time. New vertices must be inserted at the mid-span of a perimeter segment if the distance between vertices is greater than the perimeter resolution. This process has been referred to as rediscretizing (Richards 1990).

The following procedure illustrates how *FARSITE* uses the timestep and distance resolution to control a fire simulation. For a given timestep:

1. Determine the fastest spreading point on the fire front and calculate the amount of time required to spread the distance resolution (including acceleration from its current state). This will be the new *sub-timestep* required to achieve the distance resolution if it is less than the original timestep or the time interval to the next wind observation.
2. Set the dynamic timestep to this *sub-timestep*.
3. Calculate the fire growth for the *sub-timestep*.

Table 4—Fire growth simulation process control used in *FARSITE.*

```
For each timestep (date and time specified)
{       For each fire
        {       For each vertex (X, Y)
                {       Get the fire environment (fuels, weather, topography)
                        Calculate fuel moistures from initial conditions
                        Calculate vertex orientation angle (eqs. [3] [4])
                        Calculate surface fire (below)
                        if (Canopy Cover >0)
                                Calculate crown fire (below)
                }
                Correct crossovers
                Compute area and perimeter
        }
}
Ember flight, ignition, growth from time of contact
Merge all fires

Surface fire Calculations
{       Compute forward equilibrium spread rate (eq. [18])
        Vector wind and slope (eqs. [11] [12])
        Compute elliptical dimensions using resultant wind-slope vector (eqs. [13]-[17])
        Compute spread rate Rt by accelerating fire over timestep (eq. [29])
        Compute average spread rate of fire over timestep
        Compute spread differentials (eqs. [1] [2])
        Slope transformation (eqs. [8] [9])
        Compare fire spread with distance resolution
        if (fire spread is truncated to distance resolution)
        {       Compute time to spread distance resolution with acceleration (eqs. [29]-[33])
                Adjust spread distance to distance resolution
                Reduce time elapsed to accomplish distance resolution
        }
}

Crown Fire Calculations
{       Calculate Critical Surface Fire Intensity Io (eq. [21])
        if (actual surface intensity>= Io)
        {       Compute crown fraction burned (eq. [25])
                Compute acceleration constant for crown fire spread (eq. [30])
                Compute maximum crown fire spread rate (eq. [24])
                Vector open wind and slope (eqs. [11] [12])
                Compute elliptical dimensions using resultant wind-slope vector (eqs. [13]-[17])
                Compute critical crown fire spread rate (eq. [22])
                Compute actual crown fire spread rate (eq. [23])
                if (actual crown fire spread (eq. [23])>= critical crown fire spread rate (eq. [22])
                {       Accelerate crown spread rate (eq. [30])
                        Compute crown spread differentials (eqs. [1] [2])
                        Slope Transformation (eqs. [8] [9])
                        Compare fire spread to distance resolution
                        if (crown fire spread is truncated to distance resolution)
                        {       Fire acceleration as a function of distance resolution (eq. [29]-[33])
                                Adjust spread distance to distance resolution
                                Reduce time elapsed because of increased spread rate
                        }
                        Compute Crown Fire Intensity (eq. [28])
                        Ember Lofting from Active Crown Fire
                }
                else
                {       Compute Crown Fire Intensity (eq. [28])
                        Ember Lofting from Torching Trees
                }
        }
}

Spot Fire Calculations
{       Lofting
        {       Determine plume characteristics (for torching tree)
                Loft embers (eqs. [34]-[38])
        }
        Flight
        {       Iterate horizontal and vertical ember flight path (eqs. [39]-[43])
        }
        Ignition
        {       Determine if ember lands inside existing fires
                Apply Ignition Frequency
        }
}
```

4. Calculate the time remaining in the original timestep by subtracting the *sub-timestep*.
5. Repeat steps 1 through 4 until the original timestep is exhausted.

At the end of each sub-timestep each fire polygon is rediscretized to check the perimeter resolution. Richards (1990, 1995) includes a procedure to increase the density of vertices surrounding local regions of high curvature. This reduces acute angles on the fire front in areas of rapid growth by concentrating vertices and processing time on areas of high curvature. It is efficient for fire simulations in relatively homogeneous areas. In highly heterogeneous areas, the fire may encounter diverse environmental conditions along all portions of the perimeter; the fire perimeter needs to have a density of vertices sufficient to be sensitive on all flanks. Therefore the perimeter resolution used in *FARSITE* remains constant for all portions of the perimeter.

Crossovers

Although faithful in implementing the fire behavior models, the vector technique does not intrinsically distinguish burned from unburned areas. This becomes important to locally concave regions of the fire front that eventually overlap (fig. 4). If allowed to continue without detecting burned terrain, the fire front will form complex loops and knots. These *crossovers,* however, must be removed to preserve the meaningful portions of the fire front. Given the typically fine resolution of the fire front compared to the raster landscape, it is not possible merely to change landscape data to "nonfuel" as the fire front passes. Instead, perimeter vertices within a burned region must be identified computationally. Sometimes, an enclave or island is formed by a crossover. This condition represents a region of the perimeter in which the vertices are ordered in an opposite rotation. These enclaves essentially become separate fire fronts burning inward as a natural result of their orientation in equations [1] and [2] (Richards 1990).

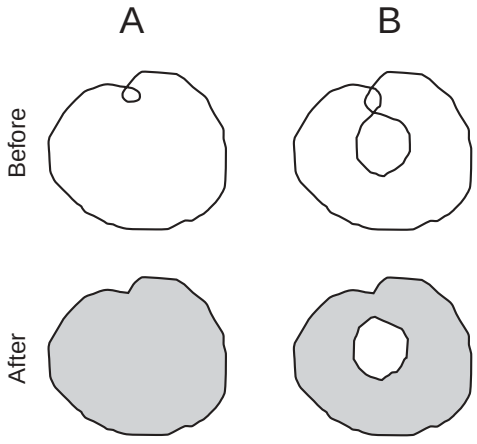

Figure 4—Correcting fire perimeter expansions is necessary because there is no inherent detection of previously burned areas. Examples of **(A)** clipping of simple crossovers or loops and **(B)** clipping illogical overlap but preserving an enclave.

Several methods have been proposed to remove illogical artifacts of the perimeter expansion. Richards (1990), Knight and Coleman (1993), and Wallace (1993) used clipping strategies to excise irrelevant portions of the fire perimeter from the fire polygon. Richards and Bryce (1995) described an algorithm that leaves the illogical perimeter vertices intact but renders them inert. The method described below is a clipping routine that enables orderly storage of only meaningful fire perimeter information and facilitates export of fire polygons for GIS uses. Regardless of the methods chosen, the process of crossover removal is expensive in time and computing power, and is an interesting area for further research and improvement.

The algorithm developed for use in *FARSITE* requires three preliminary steps. First, the fire perimeter vertices must be ordered beginning from a vertex on the outside edge of the fire polygon; this is ensured by using one of the *extreme points* (one of the polygon vertices that defines the farthest extent of the polygon along a given horizontal axis). For practicality, a vertex is selected from those that define the bounding rectangle of the polygon (farthest east, west, north, or south). Second, a list of pairwise comparisons is made to detect intersections between each perimeter segment and every other perimeter segment of a given fire polygon. If intersections are found, intersection pairs are stored in the order found and labeled by the order number of the first vertex on the crossing spans. This list contains all intersections within a polygon. Third, the intersection list is reviewed to identify multiple intersections within a given segment. Multiple intersections on a segment are reordered so that they appear in the sequence in which they would be encountered starting from the first vertex. New vertices are inserted along the segment to separate multiple intersections so that the rotational direction at the intersection can be properly identified below.

If intersections are found during the preliminary steps, the algorithm corrects the fire polygon by following the outer edge from the first vertex on the polygon. For an outward burning fire it proceeds with each perimeter segment (pair of vertices) until an intersection with another segment is encountered. Vertices between intersections are stored separately to form what will be the corrected fire polygon. When the process finds one of the intersections identified above, it decides first, the rotation direction produced by the intersection with the new perimeter segment and second, the local shape of the fire front (convex or concave). These criteria are used to determine the next vertex to be processed (either in the existing direction around the fire polygon or in the reverse direction):

	Clockwise	**Counter-Clockwise**	**Linear**
Convex	reverse direction	reverse direction	existing direction
Concave	reverse direction	existing direction	existing direction

The intersection point is stored as the next vertex on the new fire polygon. The process is continued until the algorithm arrives back at the start and determines the vertices that now define the outermost fire perimeter.

After processing the vertices for the outermost fire polygon, the algorithm looks for perimeter segments listed as crossing but not processed during the above search for the outer fire polygon. These unprocessed segments will occur if an enclave is formed. If one of these intersections is found, the intersection serves as the starting point for the same algorithm to again follow the edge of the fire polygon. This process determines if a new inward fire has been created within the original fire perimeter polygon (an enclave).

Each enclave is written as a separate fire if it has more than two vertices and is oriented clockwise. This process is repeated until there are no remaining unprocessed crosses on the original fire perimeter polygon.

Fire Mergers

Mergers between separate fire polygons must be computed if more than one fire is being simulated. Searching for fire mergers is accomplished at the end of a timestep after all fires have spread and crossovers removed. This is a computationally intensive process that first compares the bounding rectangles for each fire. If rectangles for two fires overlap, it examines segments of the first fire for intersections with those of the second fire within the overlapping region.

As with crossovers, the intersection coordinates and average fire characteristics of the intersecting segments are stored, as well as the order of segments in each fire that cross. This information is used by one of two algorithms. If there are only two crosses between fires, then no enclaves can be formed and the simpler, faster algorithm merges these fires (fig. 5a). Merging fires with more than two intersections uses the comparatively complex algorithm to write segments alternately from each fire between intersections. There can be only one outward burning fire perimeter, so all subsequent fire perimeters must be inward burning enclaves (fig. 5b).

The algorithms for merging fires will perform mergers between (1) two separate outward burning fire polygons, and (2) between an inward burning fire polygon and an outward burning polygon (fig. 5c). The latter situation develops where spot fires are burning within an inward burning polygon (that defines the fire front around an enclave). The spot fires will burn as independent fires until they merge with each other or merge with segments of the enveloping inward burning fire polygon. No situation can logically develop where two inward burning fire polygons could merge.

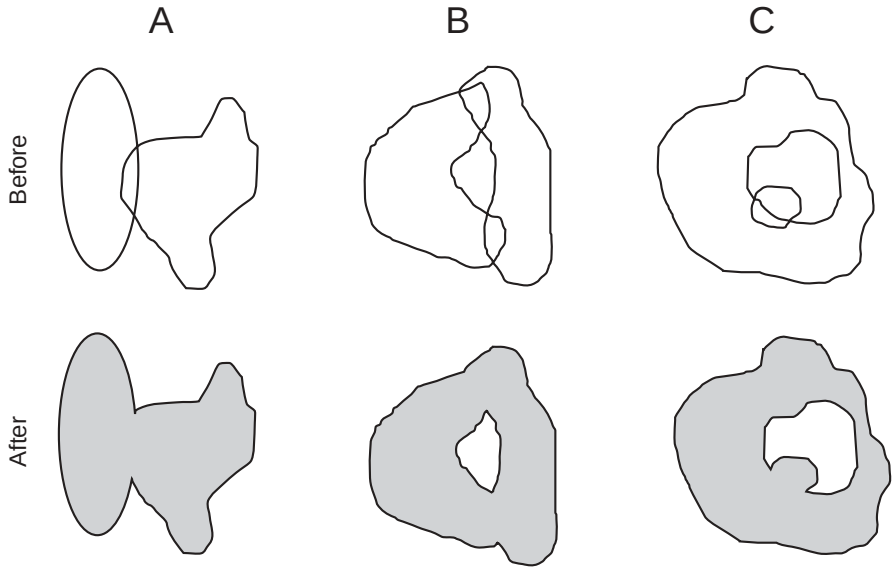

Figure 5—Examples of fire mergers. **(A)** Merger of two fires. **(B)** Merger of fires forming an enclave. **(C)** Merger of spot fire within an enclave.

The process of merging fires proceeds first with mergers among all outward burning fires, and then for mergers between enclaves and outward burning perimeters. This sequence eliminates illogical overlaps between outward burning fires that could influence how enclaves are processed when they contain spot fires.

Rasterizing and Vector Output

Fire perimeter polygons are the native output format of fire growth simulations using Huygens' principle. The vertices of the fire polygons contain information on frontal fire behavior characteristics, namely fireline intensity and spread rate, that can be interpolated for display in raster format. The interpolation is achieved at the sub-timestep level (see previous section on Control of Spatial and Temporal Resolution) to assure the minimum specified spatial and temporal resolutions of the raster maps. Time of arrival for a given raster is computed as the inverse distance weighted average of the radial distance between a given raster centroid and the fire perimeter segments (at time t and $t + \Delta t$) arriving on either side of the centroid (fig. 6). Fire behavior is interpolated from values at the four vertices that surround the raster centroid. The algorithm uses the inverse area weighting of the four component quadrilaterals formed by these four vertices and the raster centroid. The algorithm collapses to an inverse distance weighting if the centroid falls on one of the outer lines.

Simulations and Results

Test conditions were devised to provide a useful reference for interpreting fire growth simulated under more realistic but complex environmental conditions. Also, simulations were designed to demonstrate the effects of the major factors affecting fire shape and intensity patterns. Actual fire patterns are often difficult to explain because all factors vary spatially, and weather and fuel moistures vary temporally. Focusing on a few environmental variables at a time, the simulations below illustrate the role of individual factors on fire growth and behavior. They also tested the performance of component fire behavior models. Poor or unrealistic model performance could be graphically identified, pointing to weaknesses in existing data or models. Future improvements or replacements to the component fire behavior models can then be compared in terms of the effects on spatial patterns of intensity and fire growth. All simulation results are shown in plan view (projected to horizontal). Not all combinations of all factors were simulated.

Surface Fire and Windspeed

Increasing windspeeds on flat terrain resulted in elliptical fire shapes (color plate 2). The eccentricity, spread rate, and fireline intensity is determined by the strength of the wind vector. The fireline intensity patterns exhibited a radial pattern emanating from the ignition point.

Surface Fire and Wind Direction

Shifts in wind direction were reflected in the changes in fire shape and intensity patterns (color plate 3). A progressive shift in wind direction rotates the backing and heading portions of the fire and their respective intensities

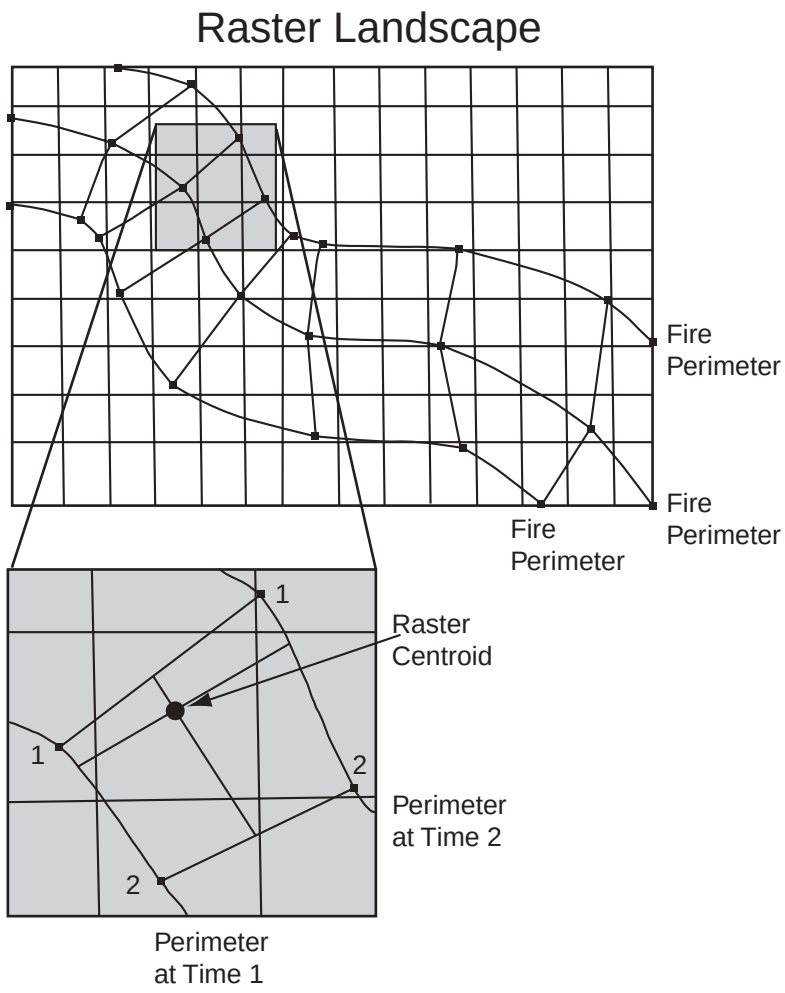

Figure 6—Method for interpolating fire behavior and time of arrival for raster centroids. Four vertices that surround a raster centroid on successive fire perimeters are used to interpolate fire behavior values.

(color plate 3a). Regular oscillations in windspeed and direction had the effect of reducing the eccentricity of an otherwise elliptical fire (color plate 3b-9e) as noted by Simard and Young (1978) and Richards (1993). A banded pattern of fireline intensities was caused by regular changes in wind direction or speed or both that temporarily reduced the fireline intensity along a portion of the perimeter (color plate 3b, 9c).

Surface Fire and Slope

Slope had several effects on the fire spread pattern (color plate 4). Surface spread was faster on steeper slopes and produced larger fires with higher intensities. Fire shapes became more eccentric along the ground surface, but that trend was not noticeable on a plan view (color plate 4). The projection of a surface fire to the horizontal view reduces the eccentricity of the fire in proportion to the cosine of slope. Thus, slope produced little change in apparent fire shapes when viewed in the horizontal.

Surface Fire and Wind and Slope

Wind and slope components are combined as vectors (color plate 5) to determine both fire spread direction, spread rate, and the elliptical dimensions (equations [11] through [17]). The symmetry of the fire shape burning in any direction was maintained on all slopes in both the horizontal and surface planes. The intensity pattern, however, did not remain symmetric in the horizontal plane when the ellipse was oriented diagonally on the slope (see color plate 5: slope 100 percent, cross-slope wind 7.5 m s^{-1}).

Fuel Change

The simulations showed the expected fire response to spatial variation in fuel types on flat terrain with constant winds (color plate 6). A patch of shrub fuel increased both intensity and spread rate (color plate 6b) and permanently altered fire shape compared to constant conditions. A rectangular patch of sparse litter fuel served as a temporary impediment to growth (color plate 6c), similar to the permanent impediment effected by the patch of nonfuel (color plate 6d).

Crown Fire

The threshold nature of transition between surface and crown fire in Van Wagner's (1977) model had a complex effect on fire shape. Color plates 7 and 8 show horizontal fire shapes ranging from fan-shaped to double ellipses depending on the wind, slope, and crown fuel parameters.

Broader crown fire shapes were facilitated by lower crown base heights and higher crown bulk densities (color plate 7). These shapes were related to the change in surface fire characteristics around the curving fire front (see surface intensity patterns in color plate 2) relative to the constant threshold levels for crown fire transition and active crowning. A lower crown base height decreases the critical surface fire intensity required for transition to crown fire (equation [21]) meaning that transition was possible from a broader surface fire front (farther back from the direction of maximum surface fire intensity). Similarly, higher crown bulk densities facilitated active crown fire by reducing the critical crown fire spread rate and permitting more of the flanking spread to exceed this threshold (equation [22]). Crown fire activity was strongly dependent on the surface fire characteristics; these, in turn, are determined by the orientation of each fire perimeter vertex.

Despite the underlying use of a simple ellipse, the shape of a point-source fire became more egg shaped when the heading portion transitioned to an actively spreading crown fire (color plate 7). After the heading surface fire became an active crown fire, its shape became more eccentric because the elliptical dimensions were determined by the faster open winds (now at "midflame" height). The understory winds reduced by canopy cover still affected the backing fire and its shape independently from the crowning portion. The active crown fire spread rate was also much faster than the surface fire, thereby increasing the crown fire size compared to its previous dimensions.

The effect of slope on crown fire shape and intensity was more variable. Under no-wind conditions, steep slopes (80 and 100 percent) led to fan-shaped fires with fairly uniform heading intensity (color plate 8). The fan shape was largely a product of the viewing perspective (the projection to the

horizontal plane) because fire spread parallel to the steep slopes is flattened by the projection. However, the assumption in this model that the slope influence on crown fire shape can be taken from that of the surface fire will need testing (see the previous subsection Vectoring Wind and Slope). On steep slopes without wind, the relatively wide angle of the heading surface fire generated a broader frontal zone with sufficient spread rate to support an active crown fire using Van Wagner's (1993) criterion (equation [22]). Increasing windspeed narrowed the fan-shaped portion by first propagating crown fire only from the narrower head of a more eccentric surface fire, and second by making the crown fire wavelet more eccentric in the windward direction.

A cross-slope wind produced asymmetric crown fire shapes (color plate 9). The asymmetry was produced because an active crown fire is assumed dependent on a supporting surface fire in Van Wagner's (1977) model. On steep slopes, the surface fire spread rate was only sufficient for supporting active crown fire in the predominantly uphill direction that results from vectoring understory wind and slope. Active crown fire spread was then deflected from the surface fire spread direction by the stronger winds used for vectoring crown fire spread direction. This directly reflects the assumptions made for wind-slope vectoring for crown fires (see previous section on Vectoring Wind and Slope). Crown fire spread in the downhill direction appeared truncated with little movement because (1) the surface fire in that direction was not spreading fast enough to support an active crown fire (equation [22] through [28]), and (2) little flanking spread is possible from the crown fire with its relatively eccentric shape determined by the faster winds. Not shown was the effect of short range spotting that would effectively increase the fire growth downwind.

Spotting

In the wind-driven fires simulated here, spotting occurred from only the heading portions of the fire because the surface intensity was high enough to initiate some form of crown fire (such as torching trees; color plate 10). Multiple spot fires created a rippled pattern of intensity that follows the spatial mixture of spread rates and directions around each spot fire. This often caused temporary enclaves to form at the juncture of multiple fires; the enclaves ultimately burned out but often with a relatively low intensity because of the presence of backing and flanking inward spread. It is important to emphasize that the simulation assumed independence of all fires and ignores potential interaction among the multiple spot fires that can occur in real fires. Alternating wind directions caused a broadening of the fire pattern because spot fires originated from embers cast only from the heading portion of the fire front. Prolific short-range spotting from passive crown fire (torching trees; color plate 10a, b) produced a fire shape similar to that of an active crown fire with or without spotting but with lower intensities (color plate 7).

Acceleration

Acceleration rates were investigated for point and line-source fires by use of a point ignition and later a 90º wind shift (color plate 11). Rapid acceleration rates allowed the fireline intensities from elliptical point-source fires to exhibit the normal radial pattern before the wind shift (color plate 11a).

Slower point-source acceleration rates, however, delayed the fires in reaching equilibrium spread rates; this produced smaller fires with V-shaped patterns of intensity that increased over time (color plate 11b,c,d). After the wind shift, the difference in response time of the forward flanks compared to the rearward lee-side flanks increased with decreasing line-source acceleration rates (the fires were no longer points). The slower spread rates of the rearward flanks prior to the wind shift required longer to accelerate toward the new equilibrium conditions imposed along those flanks by the wind shift.

Fuel Moisture

Dead fuel moisture responded on an hourly basis to the temperatures and humidities in the weather stream and affected fire growth and behavior (color plate 12). Nearly constant temperature and humidity for a given day (0600 to 2000 hrs) produced constant spread rates with the usual radial intensity pattern (color plate 12a). A typical diurnal weather pattern with changing humidity and temperature caused a decrease in fine fuel moisture at mid-day that increased fireline intensity. The trends in higher humidity and lower temperature in the afternoon and evening caused increasing fuel moistures and decreased intensities.

Discussion

The vector modeling approach proved to be a practical technique for incorporating separate models for surface fire, crown fire, acceleration, spotting, and fuel moisture. The model integration was relatively straightforward because the one-dimensional calculations for each model apply directly to the vertices on the fire front. The simulation then controls the spatial and temporal precision of all model calculations as applied over the two-dimensional landscape. The simulations represent the strict spatial consequences of the existing fire behavior models under given environmental conditions; fire behavior at each vertex is assumed to be independent of any spatial or temporal interactions involving the fire and its environment. Obviously, feedback between the fire and environment could alter fire growth patterns from those simulated here. Fire behavior that is strongly dependent on fire-environment coupling such as plume-dominated fires (Rothermel 1991), fire whorls (Byram and Martin 1970), and mass-fires (Countryman 1964) cannot be reliably modeled with this simulation.

In the simplest case, the shapes and intensity patterns of surface fires were consistent with expectations for fire growth under the ideal conditions used for wind and slope. Elliptical fires showed radiating patterns of intensity as expected from analyses by Catchpole and others (1982, 1992) when acceleration was disabled (color plate 2). By incorporating acceleration and fuel moisture changes (color plates 11 and 12, respectively), the radial pattern remained but was redistributed across space and time. The elliptical shape and intensity patterns were modifed by slope when viewed horizontally because the projection of fire growth from the surface to the horizontal flattens fire shapes in the uphill direction (color plate 4). Slope also altered the symmetry of intensity patterns as viewed from above when neither the major nor minor axis of the fire was aligned with the aspect due to wind direction (color plate 5).

The simulations of more extreme fire behavior such as crown fire and spotting could not be verified by comparison to empirical data. Data for these

types of fires are not available for the restrictive conditions of the simulations (point-source fires and essentially constant environment). Nevertheless, the crown fire simulations did reveal patterns that resemble phenomena observed on actual fires. The double ellipse model described by Anderson (1983) was essentially reproduced here by simulations of flat-terrain crown fires (color plate 7) and spotting with constant winds (color plate 10a,c). After the heading portions of a fire transition to crown fire, they were shaped by different elliptical dimensions than the rearward flanks that had remained as surface fires. This was a direct result of assuming that active crowning at the head of a fire are shaped by the open winds above the canopy that have a higher velocity than the understory winds affecting the backing fires. It is noteworthy that several fire shapes fitted by Anderson (1983) to the double ellipse were characterized by severe spotting and wind-driven crown fire runs—behavior consistent with these simulations. Spotting increased the eccentricity of the overall fire pattern by advancing embers ahead of the main fire front (produced mostly at the head and forward flanks of the fire).

Crown fire shapes without spotting were not that sensitive to variations in overstory windspeed resulting from different wind-reduction factors. Rothermel (1991) suggested a wind reduction factor of 0.5 for crown fire shapes (from the 20 ft wind) and Alexander (1985) assumed the 10 m wind was at midflame height. The apparently minimal differences may be partially explained by the truncation of the *LB* ratio to value of 8 so that higher winds simply had no more effect on shape. However, crown fires that occurred at low windspeeds (where crown bulk density and surface fire spread rate were high) also showed little sensitivity. This likely resulted because large differences still exist between windspeeds in the overstory and in the understory (reduced by stand height and canopy cover). Such different windspeeds make the heading crown fires far more eccentric than surface fires in the backing and flanking directions. Thus, when crown characteristics were sufficient to support an active crown fire, the real value used for overstory winds was relatively unimportant to the fire shape. The relatively straight-sided flanks of the crown fires in color plate 7 were somewhat a consequence of the constant wind conditions used for the simulations; more realistic conditions with an oscillating wind direction ($\pm$5 to 10°) tended to form more rounded shapes.

Other simulations produced patterns similar to the "tree-crown streets" described by Haines (1982). This term describes the visible bands of unburned tree foliage oriented parallel with the spread direction that are visible on aerial photographs (Haines 1982; Pyne 1984; Simard and others 1983; Wade and Ward 1973). Such bands are similar to the alternating zones of fireline intensity visible in the simulations of fluctuating windspeed (color plate 3b) and directions (color plate 3c). In these simulations, changing the wind direction and speed modified the intensity distribution around the fire perimeter. Within these bands, it can easily be shown using the fire behavior models here, that a sudden reduction in surface fire intensity can fail to achieve the threshold for transition to crown fire (allowing foliage to remain on trees in those bands). This explanation supports that of Alexander and others (1991) who documented the incidence of tree-crown streets and changes in wind direction recorded simultaneously. Changing wind direction also alternates the relative fire spread direction and would thereby reverse the direction of lee-side charring patterns seen on trees bordering the scorched bands (Haines 1982). This process of forming tree-crown streets

seems considerably simpler than the repeated formation of horizontal vortices (Haines 1982; Haines and Smith 1987). General characteristics of the curving intensity bands simulated by changing wind direction seems to be verified by some aerial photographs of tree-crown streets (color plate 13): (1) bands alternate from one side of the fire to the other, (2) bands are wider toward the head of the fire and narrowing to the rear, and (3) bands of low intensity are narrow because of their lower spread rates compared to wider bands of high intensity.

Patchy intensity patterns of the spot fire simulations were qualitatively similar to the variable effects within perimeters of large crown fires with prevalent spotting. Fires at Yellowstone National Park in 1988 (Despain and others 1989; Rothermel and others 1994) showed highly variable fire effects (color plate 14). Such variation can be caused directly by surface fires responding to heterogeneous weather, terrain, and surface or crown fuel structure, although the range of effects is likely to be greater under extreme conditions. Simulated fires with prolific spotting created highly variable landscape patterns because of the localized fire spread rates and directions around each spot fire. Without interaction among spot fires, each spot has a radial pattern of intensity and spread rates, similar to individual elliptical fires (color plate 2). The mergers of multiple fires often formed enclaves within the fire perimeter that eventually burned out. The spotting distances simulated here are undoubtedly too short for active crown fires. Albini's (1979) equations only apply to individual trees or discrete groups of torching trees and not a continuous crown fire front. Furthermore, the sizes of embers capable of being lofted will be underestimated for active crown fire conditions. As yet, no models exist for ember lofting or spotting from active crown fires.

Crown fire simulations also suggested weaknesses in fire behavior knowledge. In particular, the effects of wind and slope on active crown fire spread as modeled here seems suspect. The coefficients for both wind and slope effects on surface fires may not represent realistic influences on crown fires. They might, therefore, contribute to the curious fan shapes on steep slopes with low windspeeds. Nevertheless, the fan-shaped fires may not be entirely illogical. They persist even with stronger uphill winds and were similar in shape to the V-shaped pattern of head-fire intensity of elliptical fires (fig. 8, 10, 11). This was not surprising, given that the head-fire intensity is responsible for the transition of the surface fire to a crown fire. Thus, a fan shape may reflect a real geometric effect on steep slopes caused by the combination of both viewing angle (horizontal projection) and restricted uphill directions at which surface fires can transition to crown fire.

The assumed dependence of a crown fire on supporting surface fire had some odd consequences under cross-slope wind conditions (color plate 9). Here, the downhill-downwind spread was truncated below a certain radial angle (depending on the particular windspeed and slope). The surface fire was spreading too slowly in this direction to maintain an active crown fire; only limited flanking in this direction was then possible from the more eccentric active crown fire portions. Under real conditions of strong wind or high crown bulk density or both (described by Van Wagner 1977) the crown fire might be expected to move downwind independently of the surface fire for short distances and thereby mitigate this truncation effect on crown fire shape. Also, short range spotting, omitted intentionally from these simulations, would extend the burn pattern in the downwind direction from the

actively crowning perimeter. The independent contribution of each process to crown fire spread is, however, difficult to separate or document for actual crown fires. It might lead, therefore, to mismatched comparisons between observations and model results. Some of the uncertainties in the crown fire simulations may someday be clarified by the incorporation of more advanced models of crown fire spread (such as Albini and Stocks 1986). Despite the peculiarity of fire shapes in these simulations, their relevance to real fire conditions may be limited by the rarity of point-source crown fire ignitions occurring with uniform fuel, topography, or weather. Another reason this simulation model may underestimate the potential for crowning or torching is that only the flaming front is assumed to initiate combustion of the aerial fuels. Rothermel (1994) suggested that postfrontal combustion of larger woody fuels (1,000 hr+) could provide a long-duration source of radiative and convective heating capable of igniting tree crowns after the fire front has passed by.

Because the wave-front approach to fire growth modeling accommodates heterogeneous conditions in space and time, it is likely to be suitable for simulating wind-driven wildland fires if enough data are available for describing the fire environment. The few comparisons with observed fire spread patterns have shown reasonable agreement for surface fires where environmental conditions are relatively simple (Anderson and others 1982; French 1992). Wind changes produced fire spread shifts close to those observed for fires spreading in grass fuels with essentially no influence of topography. Sanderlin and Sunderson (1975) showed reasonable agreement between model predictions and observed perimeters of the Potrero wildfire (September 1973) in southern California. Some preliminary validations of *FARSITE* on surface fires have been promising where the burning conditions met the assumptions of the Rothermel (1972) spread equation (Finney 1994; Finney and Andrews *in press*; Finney and Ryan 1995). More validation is certainly necessary because the many potential sources of error can confound the comparisons. These tests have highlighted the need to consider error associated with (1) the model input data (fuels and weather), (2) the spatial and temporal resolution of the inputs, and (3) the observed fire progression maps used for comparison.

An important result of the comparisons of *FARSITE* projections with actual fires has been that spread rates for all fuel models tend to be overpredicted (Finney 1994; Finney and Ryan 1995). Sanderlin and Sunderson (1975) made some similar observations and suspected problems with relating windspeed to elliptical dimensions. Some problems may lie with inaccurate data on fuel moistures, fuel descriptions, or weather. Wind reduction factors for forested areas and lee-side topographic sheltering can undoubtedly cause errors for spread rate calculations on some parts of a landscape. However, the disparity appeared consistently during comparisons of a number of fires and could suggest a general conflict of scale between the frequency of data inputs to the simulation and the frequency of variation in real environmental conditions affecting a fire. If the scale of input data to the simulations is much coarser than that of the real environment (fuels, weather, and topography), the fire behavior equations will tend to produce equilibrium values rather than reflect the cumulative outcome of fluctuating fire behavior. Wind data are typically input at hourly or half-hourly intervals. Fuels and topography are resolved spatially to about 30 m. These scales are coarse compared to the real frequency of wind variation over a scale of

seconds, and fuels over distances of meters and fractions of meters. Constant mixtures of different fuels, each with its own characteristic spread rate, would produce a harmonic mean spread rate (Fujioka 1985; Martin 1988). High frequency wind variation keeps the fire accelerating and decelerating rather than moving steadily at a faster equilibrium rate (Albini 1982). For practical uses, the *FARSITE* model currently allows subjective spread-rate adjustment factors (Rothermel and Rinehart 1983) to be used in calibrating simulated with actual fire growth for individual fuel models. More research, however, is needed for estimating effects of high frequency variability on fire spread rates and behavior.

Even the simple conditions tested here revealed complex patterns of fire growth and behavior. Except for ember ignition, the simulation is deterministic but still results in complex patterns because the spatial and temporal processes controlling fire growth across the landscape are interdependent. The spatially variable patterns of fire behavior would likely be manifested also in patterns of different fire effects. Tree mortality (for example, Ryan and Reinhardt 1988) and crown scorch (Van Wagner 1973) are, for example, strongly related to fireline intensity. More variation in fire behavior and effects would obviously result on real landscapes where fuels, weather, and topography are heterogeneous. The advantage of having a deterministic and process driven simulation is that the patterns produced can be repeated and their causes interpreted. The opposite is true with simulations designed to reproduce complex spatial patterns of wildland fires by stochastic or fractal methodologies. Such models can emulate observed patterns by adjusting probabilities or parameters but are difficult to use in making inferences about the real processes or conditions that could produce patterns in nature.

A number of assumptions are critical to modeling fire growth. Some of these assumptions are probably not strictly met by current modeling methods. The degree to which a technical breach of these assumptions limits the practical application of a model, however, is not yet known. This is a critical question because most models will never be fully valid at all scales or for all purposes, but may be useful nonetheless if the scope of the assumptions are clearly understood. The following paragraphs present some major assumptions of the modeling method used for *FARSITE*. Andre and Viegas (1994) also detailed the subject.

1. The shapes of fires are assumed to be elliptical under uniform conditions. This assumption is justified given the mathematical simplicity of the ellipse (Van Wagner 1969) and absence of definitive data on alternative shapes (Alexander 1985; Green and others 1983). Other shapes have been reported, namely the ovoid (Peet 1967), pair of ellipses (Albini 1976; Anderson 1983), or fan-shaped (Alexander 1985; Byram 1959). Most of the disparity between the simple ellipse and alternate shapes occurs toward the rear of the fire where little area is burned compared to the heading portions. An analysis of fire shapes by Richards (1993) suggested that none of these alternative shapes could be explained simply from variations in windspeeds or directions acting on an otherwise elliptical spread pattern. Richards' methods, however, made the assumption that fire spread was independent of the shape or length of the fire front, which may not be completely supported (see below). Even if the assumption of elliptical fire shapes in continuous fuels is true, fire shapes in fuels that are not continuous at the scale relevant to mechanisms of fire propagation may not be elliptical or intuitive (Green 1983). For example, a fire may spread only in the heading direction because of wide

spacing between fuel patches and would have the shape of a rectangular strip. A similar phenomenon occurs with crown fires that can only maintain active spread at the head and become highly elongated. Fire shapes resulting from discontinuous fuels will not be adequately modeled.

2. Fire spread rate and intensity at a given vertex is assumed to be independent of fire and environmental interactions. Thus, the shape and length of the fire front and number or burning area of separate fires is assumed to have no influence on the fire behavior at any vertex. There are many situations where these assumptions do not hold. Ignition patterns used in prescribed burning (multiple ignitions, ring firing, and so forth) are designed to take advantage of fire modifications in the winds and environment in general. Field observations and analyses suggest that the length of a line fire can affect the spread rate and consequent fire shape (Cheney and others 1993; Weber 1989). Radiative heat transfer ahead of a spreading fire has long been known to depend on the shape and length of the fire front (Byram 1959). Fire behavior during mass fires or plume-dominated fires is obviously controlled by fire-environment interaction and cannot be modeled here.

3. Fire acceleration is assumed to be dependent on fuel type but independent of fire behavior. Independence from fire behavior means that a constant time period is required in a given fuel type to achieve a steady-state spread rate regardless of the environmental conditions. A single acceleration rate may not be accurate for all fuel types (McAlpine and Wakimoto 1991). Faster buildup times in uniformly fine fuels (such as grass) are expected compared to heavy fuel types (such as logging slash) and can be accommodated by changing the rate constant a_a in equations [29]-[33] for different fuel types.

4. Fires are assumed to instantly achieve the expected elliptical shape when burning conditions change (such as changes in windspeed or slope). This assumption is probably acceptable for simulations with a timestep longer than a few minutes. Laboratory experiments (McAlpine 1989) suggest that shape changes occur relatively rapidly and a short distance compared to the time and distance required for buildup in spread rate or intensity.

5. The elliptical shapes are assumed to be fuel independent, meaning the fire shape (not size) is only determined by the resultant wind-slope vector. This assumption is probably acceptable because (1) empirical relationships between windspeed and elliptical dimensions suggest shapes are common to a variety of fuel types over a wide range of ambient windspeeds (Alexander 1985), and (2) the empirical coefficients for wind and slope effects on fire spread rates used in the Rothermel spread equation are dependent on fuel bed characteristics (Rothermel 1972). These coefficients are the unit vectors used to obtain the resultant wind-slope vector. Questionable, however, are the effects of slope and wind on crown fire shape as discussed above.

6. Variation in windspeed and directions at a higher frequency than the wind stream resolution are assumed not to affect the elliptical fire shape. This is incorrect, but the importance of its effect on fire growth patterns is not yet clear. Fluctuating wind directions decrease the length to breadth ratio of an otherwise elliptical fire (Richards 1993; Simard and Young 1978). This has the effect of overpredicting the heading spread of a fire at the expense of flanking spread. Some compensation for the overpredicted heading spread will be achieved through use of spread rate adjustment factors. It is unlikely that the effects of highly variable windspeed on fire behavior can be realistically represented by simple arithmetic means because of the nonlinear response in spread rate and intensity to changing conditions.

7. The origin of an elliptical fire is assumed to be located at the rear focus of the ellipse. Most of the work using elliptical fire shapes assumes this (Alexander 1985; Anderson 1983; Andrews 1986) because it provides an implicit means to calculate the backing fire spread rate. Catchpole and others (1982), Alexander (1985), and Bilgili and Methven (1990) suggest that this assumption has not been adequately examined; using the focus as the ignition point may underpredict backing fire spread. It also decreases the fire area for small length to breadth ratios as windspeed increases (Bilgili and Methven 1990). On the other hand, using the no-wind-no-slope spread rate as the backing rate (Rothermel 1983) may overpredict spread with increasing slope or winds (Byram 1959). Van Wagner (1988) and Cheney (1981) show that backing spread decreases as slope inclines to about 20+ degrees. In effect, spread may be faster down steeper slopes because of ignition by rolling or sliding debris.

8. The spread of a continuous fire front can be approximated using a finite number of points. This assumption appears valid for surface fires in the relatively homogeneous conditions simulated here. Higher perimeter resolutions are probably required to reflect greater environmental heterogeneity and for simulating crown fire because of its dependence on thresholds of surface fire behavior that are strongly affected by the local shape of the fire front. The adequacy of this assumption for simulating any fire is dependent on the spatial resolution of the simulation relative to (1) the detail required by the user and (2) the spatial resolution of the data used in the simulation. Presumably a resolution can be specified that preserves the "important" features of fire growth but ignores irrelevant spatial detail. This is dependent on the purpose and requirements for the simulation. The same concept is implicit in maps of fire growth made by direct observation; minor variations in fire position that result from rocks or small discontinuities in fuel are ignored. The relevant resolution probably decreases as the fire gets larger. The finest resolution used for the simulation must be dependent on the resolution of spatial data grids used as input. Using a very fine resolution compared to the native raster resolution for fuels and topography results in an artificial or spurious level of precision. For example, using a spatial resolution of 5 m with rasters at 30 m gives a fire shape that interprets literally all of the square boundaries between different fuel types.

Conclusions

The vector approach to fire growth modeling holds promise for simulating wind-driven wildland fires using the current fire behavior models. The simulations illustrated that time-and-space dependent fire behavior can be simulated with realistic consequences to spatial patterns of fire growth and behavior. Future work needs to concentrate on validating *FARSITE* using observed fire growth patterns in a number of fuels and weather conditions. There is much room for improvement in fire growth simulation. Aside from incorporating more sophisticated fire behavior models, other dimensions of fire behavior and effects can be included. For example, postfrontal combustion and smoke production, holdover of fire activity in different fuel complexes after precipitation, live fuel moisture variation, use of harmonic mean spread rates for spatial fuel mixtures, and gridded weather and wind inputs would allow a more comprehensive simulation of fire growth and behavior.

References

Albini, F.A. 1976. Estimating wildfire behavior and effects. USDA For. Serv. Gen. Tech. Rep. INT-30.

Albini, F.A. 1979. Spot fire distance from burning trees—a predictive model. USDA For. Serv. Gen. Tech. Rep. INT-56.

Albini, F.A. 1982. The variability of wind-aided free-burning fires. Comb. Sci. Tech. 31:303-311.

Albini, F.A. and R.G. Baughman. 1979. Estimating windspeeds for predicting wildland fire behavior. USDA For. Serv. Res. Pap. INT-221.

Albini, F.A. and B.J. Stocks. 1986. Predicted and observed rates of spread of crown fires in immature jack pine. Comb. Sci. and Tech. 48:65-76.

Alexander, M.E. 1985. Estimating the length-to-breadth ratio of elliptical forest fire patterns. pp. 287-304 Proc. 8th Conf. Fire and Forest Meteorology.

Alexander, M.E. 1988. Help with making crown fire hazard assessments. In: Fischer, W.C. and S.F. Arno (compilers), Protecting people and homes from wildfire in the Interior West. USDA For. Serv. Gen. Tech. Rep. INT-251. pp. 147-156.

Alexander, M.E., N.P. Cheney, and A.C.F. Trevitt. 1991. Tree-crown streets and wildfires in pine plantations of Australasia. Proc. 11th Conf. Fire and Forest Meteorology, p. 167.

Anderson, D.H, E.A. Catchpole, N.J. DeMestre, and T. Parkes. 1982. Modeling the spread of grass fires. J. Austral. Math. Soc. (Ser. B.) 23:451-466.

Anderson, H.E. 1982. Aids to determining fuel models for estimating fire behavior. USDA For. Serv. Gen. Tech. Rep. INT-122.

Anderson, H.E. 1983. Predicting wind-driven wildland fire size and shape. USDA For. Serv. Res. Pap. INT-305.

Andre, J.C.S. and D.X. Viegas. 1994. A strategy to model the average fireline movement of a light to medium intensity surface forest fire. Proc. 2nd Intl. Conf. Forest Fire Research, Coimbra 1994. pp. 221-242.

Andrews, P.L. 1986. BEHAVE: fire behavior prediction and fuel modeling system- BURN subsystem, Part 1. USDA For. Serv. Gen. Tech. Rep. INT-194.

Beck, J.A. and A.C.F. Trevitt. 1989. Forecasting diurnal variations in meteorological parameters for predicting fire behavior. Can. J. For. Res. 19:791-797.

Beer, T. 1990. The Australian National Bushfire Model Project. Mathl. Comput. Modeling 13(12):49-56.

Beer, T. and I.G. Enting. 1990. Fire spread and percolation modelling. Mathl. Comput. Modeling 13(11):77-96.

Bilgili, E. and I.R. Methven. 1990. The simple ellipse: A basic growth model. 1st Intl. Conf. on Forest Fire Research, Coimbra 1990. pp. B.18-1 to B.18-14.

Blackmarr, W.H. 1972. Moisture content influences ignitability of slash pine litter. USDA For. Serv. Res. Note SE-173.

Bradshaw, L.S, J.E. Deeming, R.E. Burgan, and J.D. Cohen. 1984. The 1978 National Fire-Danger rating system: Technical Documentation. USDA For. Serv. Gen. Tech. Rep. INT-169.

Bratten, F.W. 1978. Containment tables for initial attack on forest fires. Fire Tech. 14(4) 297-303.

Bunting, S.C. and H.A. Wright. 1974. Ignition capabilities of non-flaming firebrands. J. For. 646-649.

Burgan, R.E. 1987. Concepts and interpreted examples in advanced fuel modeling. USDA For. Serv. Gen. Tech. Rep. INT-238.

Burgan, R.E. and R.C. Rothermel. 1984. BEHAVE: Fire behavior prediction and fuel modeling system - FUEL subsystem. USDA For. Serv. Gen. Tech. Rep INT-167.

Byram, G.M. 1959. Chapter Three, Combustion of Forest Fuels. In: Davis, .K.P., Forest Fire: Control and Use. McGraw-Hill. New York.

Byram, G.M. and R.E. Martin. 1970. The modeling of fire whirlwinds. For. Sci. 16(4):386-399.

Catchpole, E.A., M.E. Alexander, and A.M. Gill. 1992. Elliptical-fire perimeter- and area-intensity distributions. Can. J. For. Res. 22:968-972.

Catchpole, E.A, N.J. DeMestre, and A.M. Gill. 1982. Intensity of fire at its perimeter. Aust. For. Res. 12:47-54.

Cheney, N.P. 1981. Fire Behavior. In: Gill, A.M., R.H. Groves, and I.R. Noble (eds.) Fire and the Australian biota. Aust. Acad. Science. Canberra.

Cheney, N.P. and J.S. Gould. 1997. Letter to the editor: fire growth and acceleration. Intl. J. Wildl. Fire 7(1):1-6.

Cheney, N.P., J.S. Gould, and W.R. Catchpole. 1993. The influence of fuel, weather, and fire shape variables on fires-spread in grasslands. Intl. J. Wildl. Fire 3(1):31-44.

Clark, T.L., M.A. Jenkins, J.L. Coen, and D.R. Packham. 1996a. A coupled atmospheric-fire model: convective feedback on fireline dynamics. J. App. Met. 35:875-901.

Clark, T.L., M.A. Jenkins, J.L. Coen, and D.R. Packham. 1996b. A coupled atmosphere-fire model: role of the convective Froude number on dynamic fingering. Intl. J. Wildl. Fire 6(4):177-190.

Clarke, K.C., J.A. Brass, and P.J. Riggan. 1994. A cellular automaton model of wildfire propagation and extinction. Photogrammetric Eng. and Remote Sensing 60(11):1355-1367.

Colemen, J.R. and A.L. Sullivan. 1996. A real-time computer application for the prediction of fire spread across the Australian landscape. Simulation 67 (4):230-240.

Countryman, C.M. 1964. Mass fires and fire behavior. USDA For. Serv. Res. Pap. PSW-19.

Despain, D., A. Rodman, P. Schullery, and H. Shovic. 1989. Burned area survey of Yellowstone National Park: the fires of 1988. Unpublished report, Division of Research, Yellowstone National Park.

Dorrer, G.A. 1993. Modelling forest fire spreading and suppression on basis of Hamilton mechanics methods. In: G.A. Dorrer (ed). Scientific Siberian A: special issue Forest Fires Modelling and Simulation. pp. 97-116.

Feunekes, U. 1991. Error analysis in fire simulation models. M.S. thesis, University of New Brunswick, Fredericton.

Finney, M.A. 1994. Modeling the spread and behavior of prescribed natural fires. Proc. 12th Conf. Fire and Forest Meteorology, pp. 138-143.

Finney, M.A. and P.L. Andrews. [In press]. The *FARSITE* fire area simulator: fire management applications and lessons of summer 1994. Proc. Intr. Fire Council Mtg. November 1994, Coer D'Alene ID.

Finney, M.A. and K.C. Ryan. 1995. Use of the *FARSITE* fire growth model for fire prediction in US National Parks. Proc. The International Emergency Mgt. and Engineering Conf. May 1995 Sofia Antipolis, France. pp. 183-189.

Forestry Canada Fire Danger Group. 1992. Development and structure of the Canadian Forest Fire Behavior Prediction System., Inf. Rep. ST-X-3.

French, I.A. 1992. Visualisation techniques for the computer simulation of bushfires in two dimensions. M.S. thesis, University of New South Wales, Australian Defence Force Academy, 140 p.

French, I.A., D.H. Anderson, and E.A. Catchpole. 1990. Graphical simulation of bushfire spread. Math. Comput. Model. 13(12): 67-71.

Fujioka, F.M. 1985. Estimating wildland fire rate of spread in a spatially nonuniform environment. For. Sci. 31(1):21-29.

Green, D.G. 1983. Shapes of simulated fires in discrete fuels. Ecol. Mod. 20:21-32

Green, D.G., A.M. Gill, and I.R. Noble. 1983. Fire shapes and the adequacy of fire-spread models. Ecol. Mod. 20:33-45.

Hartford, R.A. and R.C. Rothermel. 1991. Moisture measurements in the Yellowstone Fires in 1988. USDA For. Serv. Res. Note INT-396.

Haines, D.A. 1982. Horizontal roll vortices and crown fires. J. Appl. Meteor. 21:751-763.

Haines, D.A. and M.C. Smith. 1987. Three types of horizontal roll vortices observed in wildland mass and crown fires. J. Clim. Appl. Meterol. 26:1624-1637.

Johansen, R.W. 1987. Ignition patterns and prescribed fire behavior in southern pine forests. Georgia For. Comm. For. Res. Pap. 72.

Karafyllidis, I. and A. Thanailakis. 1997. A model for predicting forest fire spreading using cellular automata. Ecol. Mod. 99: 87-97.

Knight, I. and J. Coleman. 1993. A fire perimeter expansion algorithm based on Huygens' wavelet propagation. Int. J. Wildl. Fire 3(2): 73-84.

Kourtz, P, S. Nozaki and W. O'Regan. 1977. Forest fires in the computer—A model to predict the perimeter location of a forest fire. Fisheries and Environment Canada. Inf. Rep. FF-X-65.

Kourtz, P. and W.G. O'Regan. 1971. A model for a small forest fire…to simulate burned and burning areas for use in a detection model. For. Sci. 17(2):163-169.
Linn, R. 1997. A transport model for prediction of wildfire behavior. LA-13334-T Thesis, Los Alamos National Laboratory.
Martin, R.E. 1988. Rate of spread calculation for two fuels. West J. Appl. For. 3(2):54-55.
McArthur, A.G. 1966. Weather and grassland fire behavior. Commonw. Aust. Dept. Natl. Develop. For. and Timber Bureau Leafl. 100, 23p.
McAlpine, R.S. 1989. Temporal variations in elliptical forest fire shapes. Can J. For. Res. 19:1496-1500.
McAlpine, R.S. and R.H. Wakimoto. 1991. The acceleration of fire from point source to equilibrium spread. For. Sci. 37(5): 1314-1337.
Muraszew, A. and J.B. Fedele. 1976. Statistical model for spot fire hazard. Aerospace Report ATR-77(7588)-1. Engineering Science Operations, The Aerospace Corporation, El Segundo, CA. Report to USDA For. Serv. Riverside Forest Fire Laboratory, PSW Grand No. 22.
O'Regan, W.G., P. Kourtz, and S. Nozaki. 1976. Bias in the contagion analog to fire spread. For. Sci. 2(1):61-68.
Peet, G.B. 1967. The shape of mild fires in Jarrah forest. Austr. For. 31(2):121-127.
Pyne, S.J. 1984. Introduction to wildland fire: Fire management in the United States. John Wiley and Sons, Inc., New York. 455 p.
Richards, G.D. 1988. Numerical simulation of forest fires. Int. J. Numerical Methods in Engineering 25:625-633.
Richards, G.D. 1990. An elliptical growth model of forest fire fronts and its numerical solution. Int. J. Numer. Meth. Eng. 30: 1163-1179.
Richards, G.D. 1993. The properties of elliptical wildfire growth for time dependent fuel and meteorological conditions. Comb. Sci. Tech. 92:145-171.
Richards, GD. 1995. A general mathematical framework for modeling two-dimensional wildland fire spread. Int. J. Wildl. Fire. 5(2): 63-72.
Richards, GD. and R.W. Bryce. 1995. A computer algorithm for simulating the spread of wildland fire perimeters for heterogeneous fuel and meteorological conditions. Int. J. Wildl. Fire. 5(2):73-80.
Roberts, S. 1989. A line element algorithm for curve flow problems in the plane. CMA-R58-89. Centre for Mathematical Analysis, Aust. Nat. Univ. (Cited from French 1992).
Rothermel, R.C. 1972. A mathematical model for predicting fire spread in wildland fuels. USDA For. Serv. Res. Pap. INT-115.
Rothermel, R.C. 1983. How to predict the spread and intensity of forest and range fires. USDA For. Serv. Gen. Tech. Rep. INT-143.
Rothermel, R.C. 1991. Predicting behavior and size of crown fires in the northern Rocky Mountains. USDA For. Serv. Res. Pap. INT-438.
Rothermel, R.C. 1994. Some fire behavior modeling concepts for fire management systems. In: Proc. 12th conf. Fire and Forest Meteorology, pp. 164-171.
Rothermel, R.C., R.A. Hartford, and C.H. Chase. 1994. Fire growth maps for the 1988 Greater Yellowstone Area Fires. USDA For. Serv. Gen. Tech. Rep. INT-304.
Rothermel, R.C. and G.C. Rinehart. 1983. Field procedures for verification and adjustment of fire behavior predictions. USDA For. Serv. Gen. Tech. Rep. INT-142.
Rothermel, R.C, R.A. Wilson, G.A. Morris, and S.S. Sackett. 1986. Modeling moisture content of fine dead wildland fuels input to the BEHAVE fire prediction system. USDA For. Serv. Res. Pap. INT-359.
Ryan, K.C. and E.D Reinhardt. 1988. Predicting postfire mortality of seven western conifers. Can. J. For. Res. 18:1291-1297.
Sanderlin, J.C. and J.M. Sunderson. 1975. A simulation for wildland fire management planning support (FIREMAN): Volume II. Prototype models for FIREMAN (PART II): Campaign Fire Evaluation. Mission Research Corp. Contract No. 231-343, Spec. 222. 249 p.
Sanderlin, J.C. and R. J. Van Gelder. 1977. A simulation of fire behavior and suppression effectiveness for operation support in wildland fire management. In: Proc. 1st Int. Conv. on mathematical modeling, St. Louis, MO. pp. 619-630.
Simard, A.J., D.A. Haines, R.W. Blank, and J.S. Frost. 1983. The Mack Lack fire. USDA For. Serv. Gen. Tech. Rep. NC-83.
Simard, A.J. and A. Young. 1978. AIRPRO and airtanker productivity simulation model. Environ. Can., Can. For. Serv., For. Fire Res. Inst. Info. Rep. FF-X-66.
Van Wagner, C.E. 1969. A simple fire growth model. Forestry Chron. 45:103-104.
Van Wagner, C.E. 1973. Height of crown scorch in forest fires. Can J. For. Res. 3:373-378.
Van Wagner, C.E. 1977. Conditions for the start and spread of crownfire. Can. J. For. Res. 7:23-34.
Van Wagner, C.E. 1988. Effect of slope on fires spreading downhill. Can. J. For. Res. 18:818-820.
Van Wagner, C.E. 1989. Prediction of crown fire behaviour in conifer stands. In: MacIver, D.C, H. Auld, and R. Whitewood eds., proc. 10th conf. on fire and forest meteorology. Ottawa, Canada.
Van Wagner, C.E. 1993. Prediction of crown fire behavior in two stands of jack pine. Can. J. For. Res. 23:442-449.
Von Niessen, W. and A. Blumen. 1988. Dynamic simulation of forest fires. Can. J. For. Res. 18:805-812.
Wade, D.D. and D.E. Ward. 1973. An analysis of the Air Force Bomb Range Fire. USDA For. Serv. Res. Pap. SE-105.
Wallace, G. 1993. A numerical fire simulation model. Intl. J. Wildl. Fire 3(2):111-116.
Weber, R.O. 1989. Analytical models for fire spread due to radiation. Combust. Flame 78:398-408.
Wilson, R. 1980. Reformulation of forest fire spread equations in SI units. USDA For. Serv. Res. Note INT-292.
Xu, J. and R.G. Lathrop. 1994. Geographic information system based wildfire spread simulation. Proc. 12th Conf. Fire and Forest Meteorology, pp. 477-484.

Appendix A: List of Symbols

Symbol	Meaning
α	orientation angle of fire perimeter segment (radians), eq. [7]
β, β_{op}	packing ratio, optimum packing ratio, dimensionless, eqs. [11][12]
δ	angle difference (radians) between α and topographic aspect ω, eq. [6]
ε	effective heating number, dimensionless, eq. [18]
ϕ	topographic slope (radians) eqs. [5][6][11]
π	symbol for pi (3.141592…)
θ	direction of maximum spread rate (radians), vector of wind and slope, eq. [1][2]
ρ_a	density of air (g cm^{-3}) eq. [41]
ρ_b	ovendry fuel bulk density (kg m^{-3}) eq. [18]
ρ_s	density of charred wood (g cm^{-3}) eq. [41]
σ	surface area to volume ratio (m^{-1}) eq. [20]
ω	topographic aspect (radians) eqs. [3]-[9]
Φ_s	slope coefficient for surface fire spread (dimensionless) eq. [11]
Φ_w	wind coefficient for surface fire spread (dimensionless) eq. [12]
ξ	propagating flux ratio (dimensionless) eq. [18]
a	elliptical dimension, eqs. [1][2][15], figure 2
a_a	acceleration constant for fire spread rates, eqs. [29]-[33]
a_c	scaling coefficient for crown fraction burned, eqs. [25][26]
a_x	constant for spotting model, eq. [34]
b	elliptical dimension, eqs. [1][2][16], figure 2
b_x	constant for spotting model, eq. [34]
c	elliptical dimension, eqs. [1][2][17], figure 2
f	filling fraction of forest canopy, eqs. [44][45]
g	acceleration of gravity, eqs. [40][41]
h	heat yield of fuel (kJ kg^{-1}) eq. [19]
r	complex constant used for spotting model, eqs. [36]-[38]
w	ovendry weight of fuel consumed in flaming front (kJ m^{-2}) eq. [19]
t_f	duration of flame flow structure from torching tree (dimensionless) eq. [34]
t_t	total travel time for ember (dimensionless)
t_o	time of steady burning of tree crowns (dimensionless) eq. [35]
t_1	time for ember to travel up to tip of flame (dimensionless) eqs. [35][36]
t_2	time for ember to travel through transition zone (dimensionless) eqs. [35][37]
t_3	time for ember to travel to tip of buoyant plume (dimensionless) eqs. [35][38]
v_o	terminal velocity of ember particle (m s^{-1}), eqs. [36]-[38]
w_F	flame gas velocity (m s^{-1}) eqs. [36][38]
x_s	angle differential in horizontal x-dimension (radians) eqs. [1]-[4]
y_s	angle differential in horizontal y-dimension (radians) eqs. [1]-[4]
z	particle height (m) eq. [34]
z_F	flame height (m) eq. [34]
B	constant for spotting model, eqs. [36][38]
C	canopy cover (percent) eq. [44]
C_D	drag coefficient (dimensionless) eq. [41]
CFB	crown fraction burned, eqs. [23][25][28]

D	fire spread distance, with acceleration, spread rate, and time (m) eq. [31]
D_p	ember particle diameter (m) eq. [37]
D_i	difference of horizontal and surface distance of fire perimeter (m) eqs. [3]-[5]
D_r	difference of horizontal and surface distance of fire spread rate (m) eqs. [8]-[10]
D_t, D_{t+1}	spread distance required to achieve a given spread rate with acceleration eq. [32]
E_i	fraction of forward active crown fire spread rate, eq. [24]
E, E_o	actual and critical energy flux for independent crown fires
H	forest crown height (m) eqs. [42][43][44]
HB	head to back ratio for elliptical fire shape, eq. [14]
I_b	fireline intensity (kW m^{-1}) eq. [20]
I_c	fireline intensity of a crown fire (kW m^{-1}) eq. [28]
I_o	critical intensity for initiation of crown fire (kW m^{-1}) eq. [21]
K	constant for spotting model eq. [40]
LB	length to breadth ratio for elliptical fire shape, eq. [13]
R	surface fire spread rate (m min^{-1}) eqs. [18-20][23][27][29][31][32]
RAC	critical crown fire spread rate for active crown fire (m min^{-1}) eq. [22]
$R_{Cactual}$	actual active crown fire spread rate (m min^{-1}) eq. [23]
R_{Cmax}	maximum active crown fire spread rate (m min^{-1}) eqs. [23][24]
R_o	critical crown fire spread rate associated with I_o (m min^{-1}) eqs. [25][27]
R_t	fire spread rate at time t, with acceleration (m min^{-1}) eqs. [29][33]
M	foliar moisture content (percent) eq. [21]
T_t	time (min) required to achieve the current spread rate with acceleration, eq. [33]
U_c	windspeed at "midflame" height (m s^{-1}) eq. [44]
U_h	windspeed at height h (m s^{-1}) eq. [42]
X_t	surface spread rate component for x-dimension (m min^{-1}) eq. [1]
Y_t	surface spread rate component for y-dimension (m min^{-1}) eq. [2]
X_t'	horizontal spread rate component for x-dimension (m min^{-1}) eq. [8]
Y_t'	horizontal spread rate component for y-dimension (m min^{-1}) eq. [9]

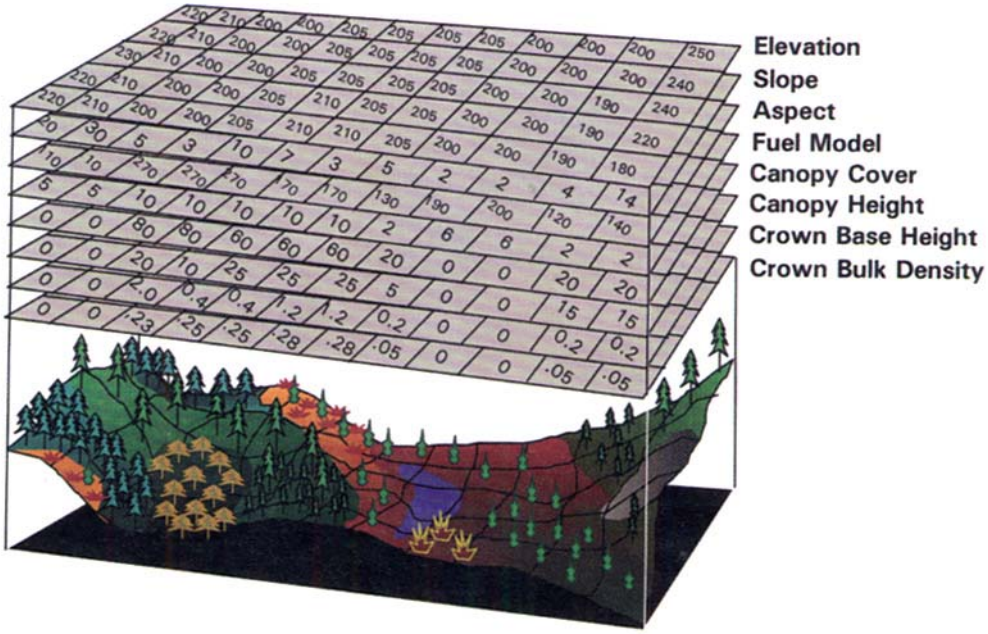

Color plate 1—Raster landscape input layers required from the GIS for *FARSITE* simulation.

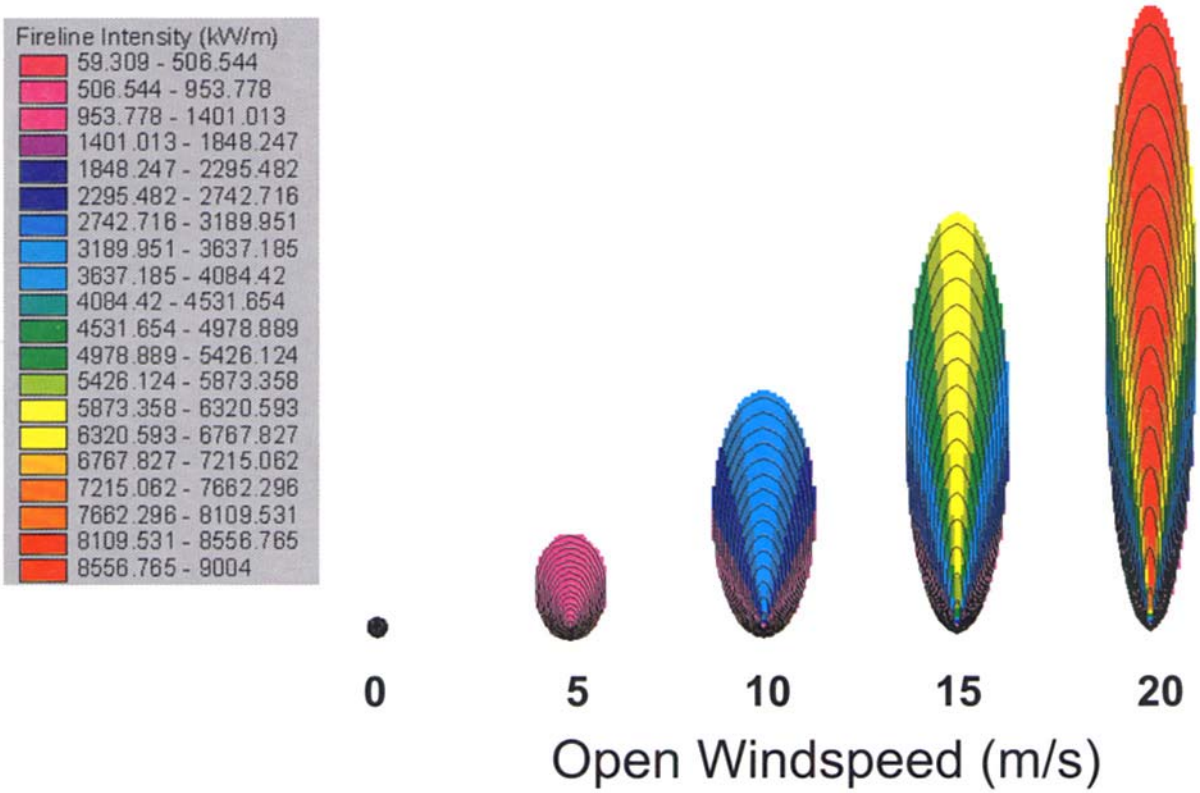

Color plate 2—Elliptical surface fire shapes on flat topography with varying windspeeds. No acceleration, visible timestep 2.0 minutes.

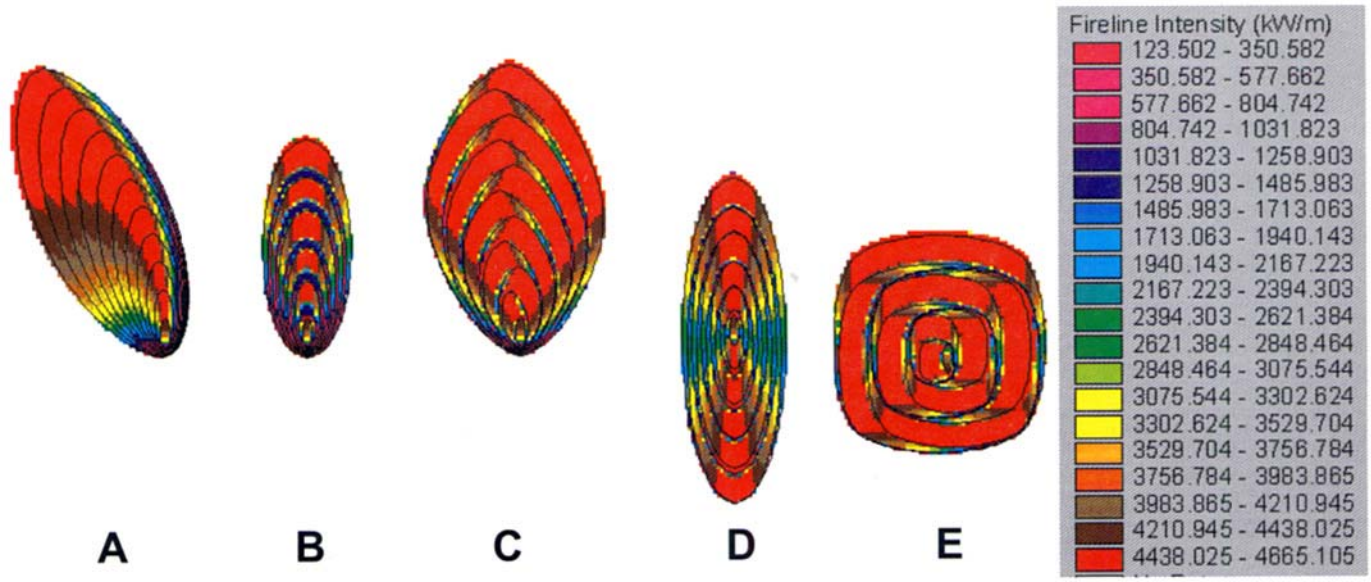

Color plate 3—Surface fire shapes and intensity patterns as affected by shifting winds on flat topography. **(A)** Constant speed with gradual shift to easterly winds. **(B)** South wind with alternating speeds. **(C)** Constant speed with alternating directions (40 degrees from south) at a constant interval. **(D)** Alternating directions (180 degrees). **(E)** Counter-clockwise rotating wind direction at constant interval. Visible timestep 5.0 minutes, no acceleration.

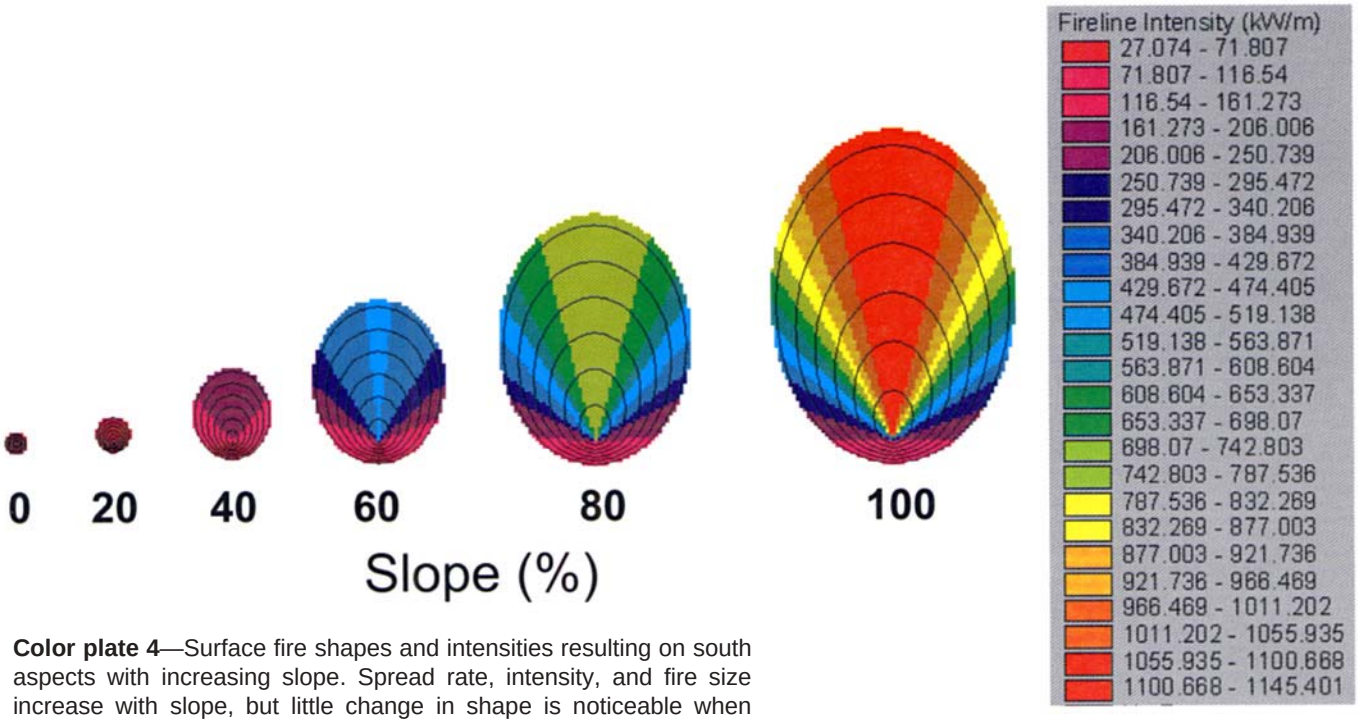

Color plate 4—Surface fire shapes and intensities resulting on south aspects with increasing slope. Spread rate, intensity, and fire size increase with slope, but little change in shape is noticeable when projected to the horizontal plane. Visible timestep 5.0 minutes, no acceleration.

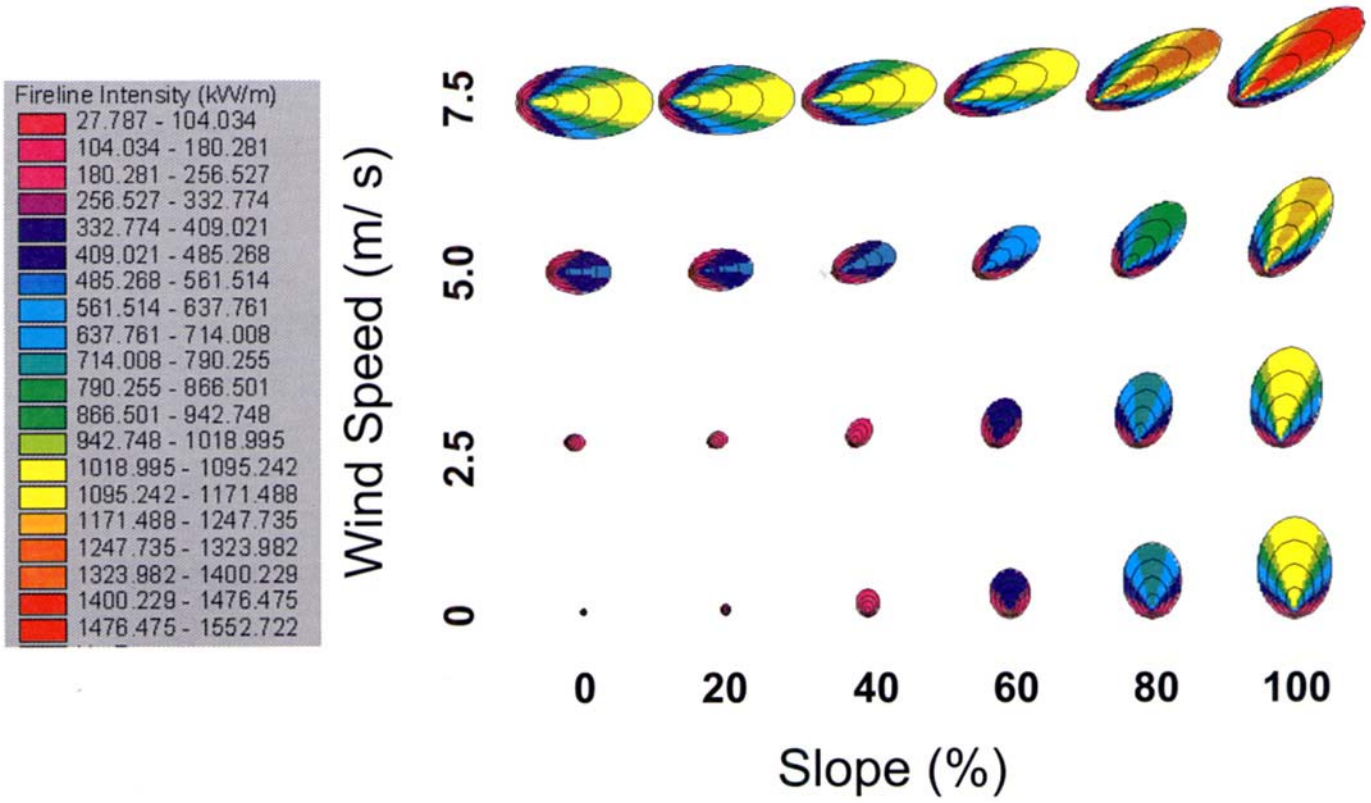

Color plate 5—Surface fire shapes and intensity patterns resulting with vectored cross-slope winds (south facing slope and west winds). The asymmetric intensity patterns that develop under higher wind-speeds and steeper slopes are a consequence of the horizontal projection. Visible timestep 5 minutes, no acceleration.

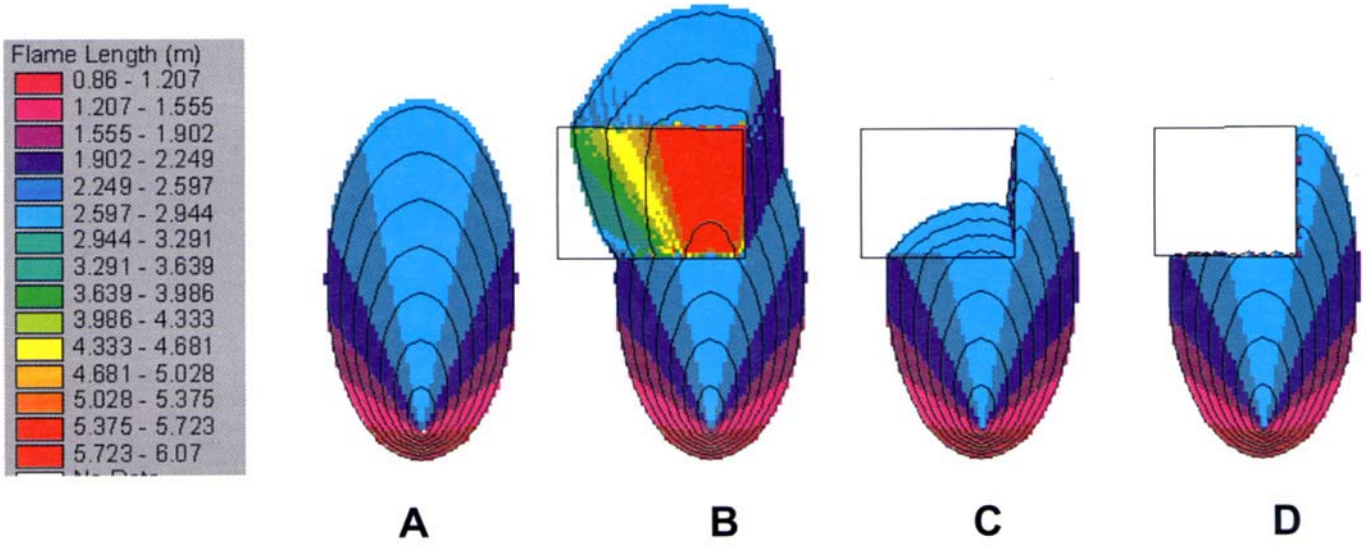

Color plate 6—Surface fire shapes and intensity patterns change when the fire encounters fuel type changes on flat topography and 7 m s^{-1} open windspeed. **(A)** No fuel change. **(B)** Block of faster fuel. **(C)** Block of slower fuel. **(D)** Block of nonfuel. Visible timestep 5 minutes, no acceleration.

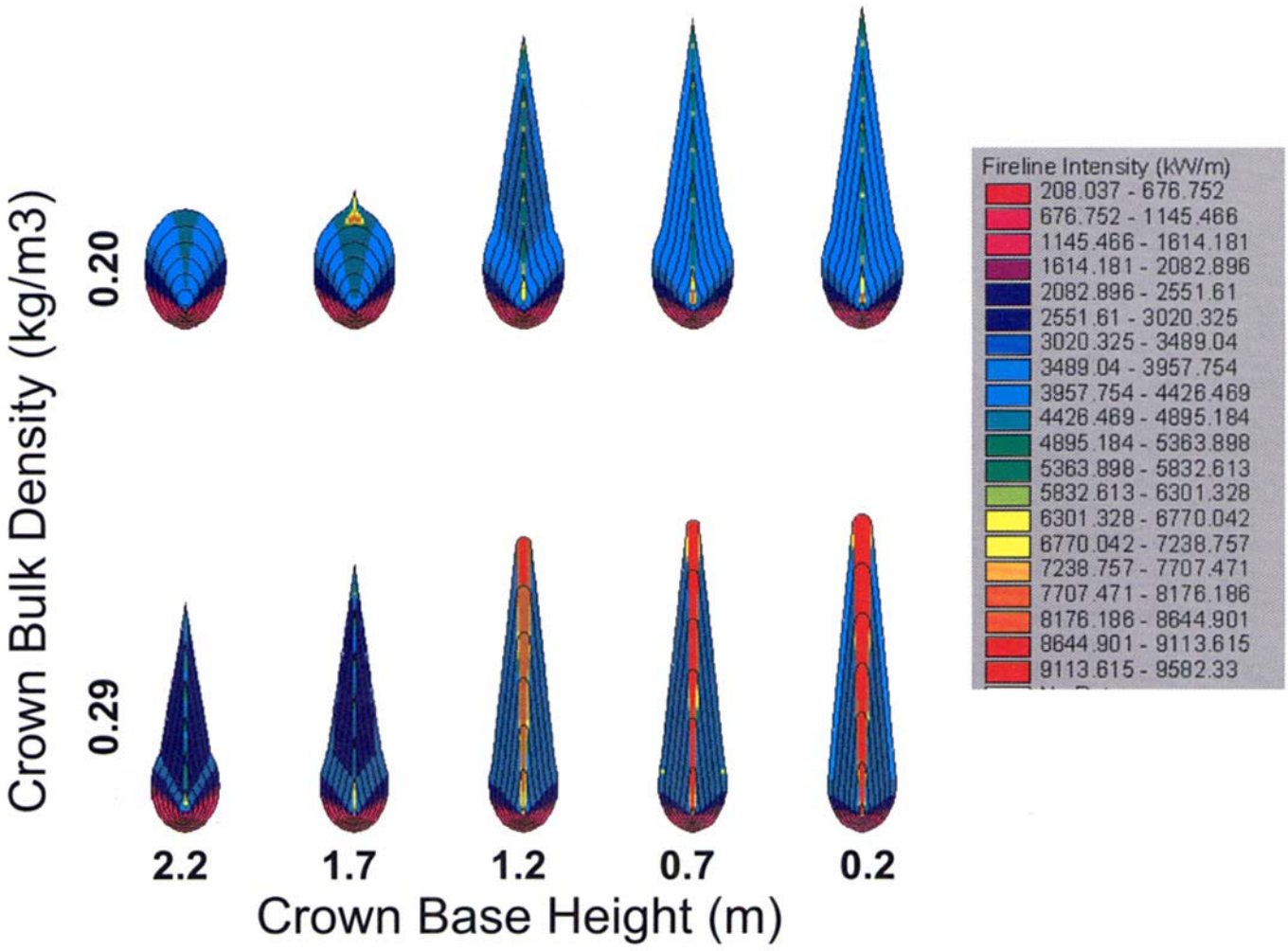

Color plate 7—Crown fire patterns on flat terrain as a function of crown base height and crown bulk density (canopy cover 75 percent for all fires). Decreasing crown base height facilitates transition to crown fire from a broader portion of the fire front. Increasing crown bulk density facilitates active crowning by relaxing the threshold for a critical crown fire spread rate. Visible timestep 2 minutes, no acceleration, wind speed 15 m s^{-1}.

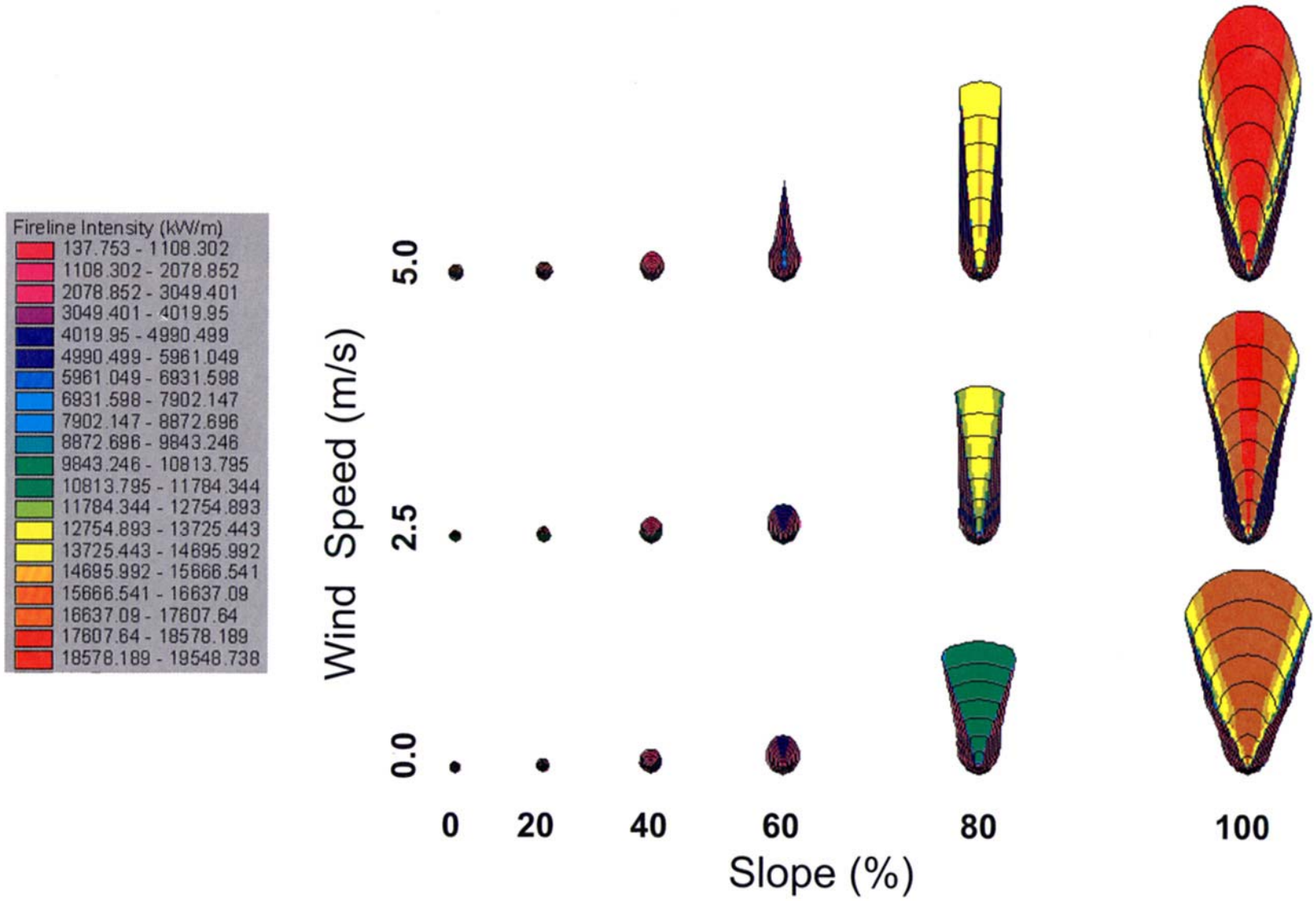

Color plate 8—Crown fire patterns as a function of slope and uphill windspeed. Fan-shaped fires result on steep slopes because of the horizontal projection and relatively minor slope effect on fire shape. Visible timestep 5 minutes, no acceleration, surface fuel model 10, crown height = 15 m, canopy cover = 70 percent, crown bulk density = 0.25 kg m^{-3}, crown base height = 2.5 m.

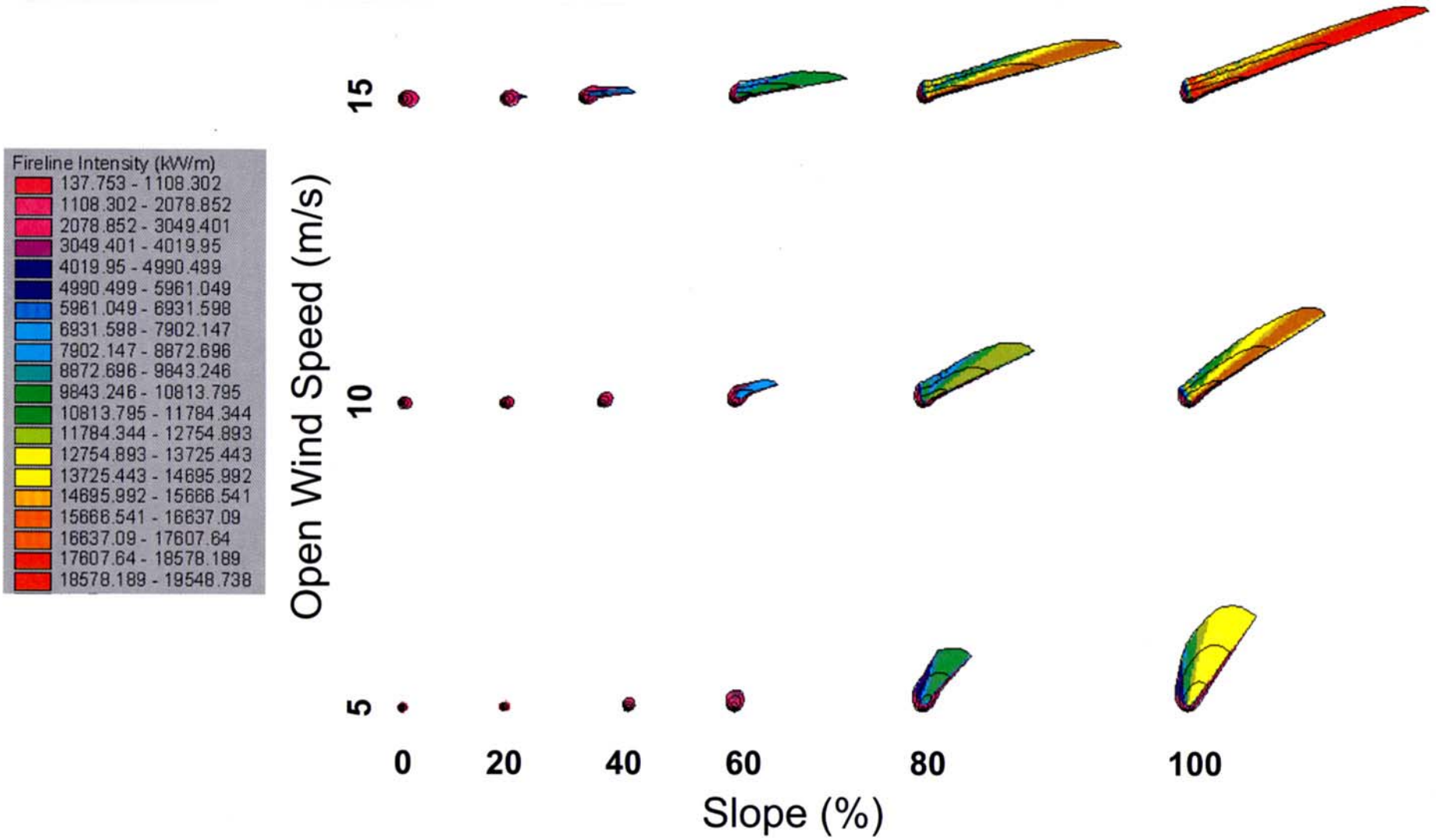

Color plate 9—Crown fires modified by west winds across south-facing slopes. Active crownfire is maintained only at the head of surface fires and then deflected by the open winds. Asymmetry of crownfire results because the crownfire model requires continual support from surface fire that only has sufficient spread rate in the vectored uphill direction. No acceleration, surface fuel model 10, crown height = 15 m, canopy cover = 70 percent, crown bulk density = 0.25 kg m^{-3}, crown base height = 2.5 m.

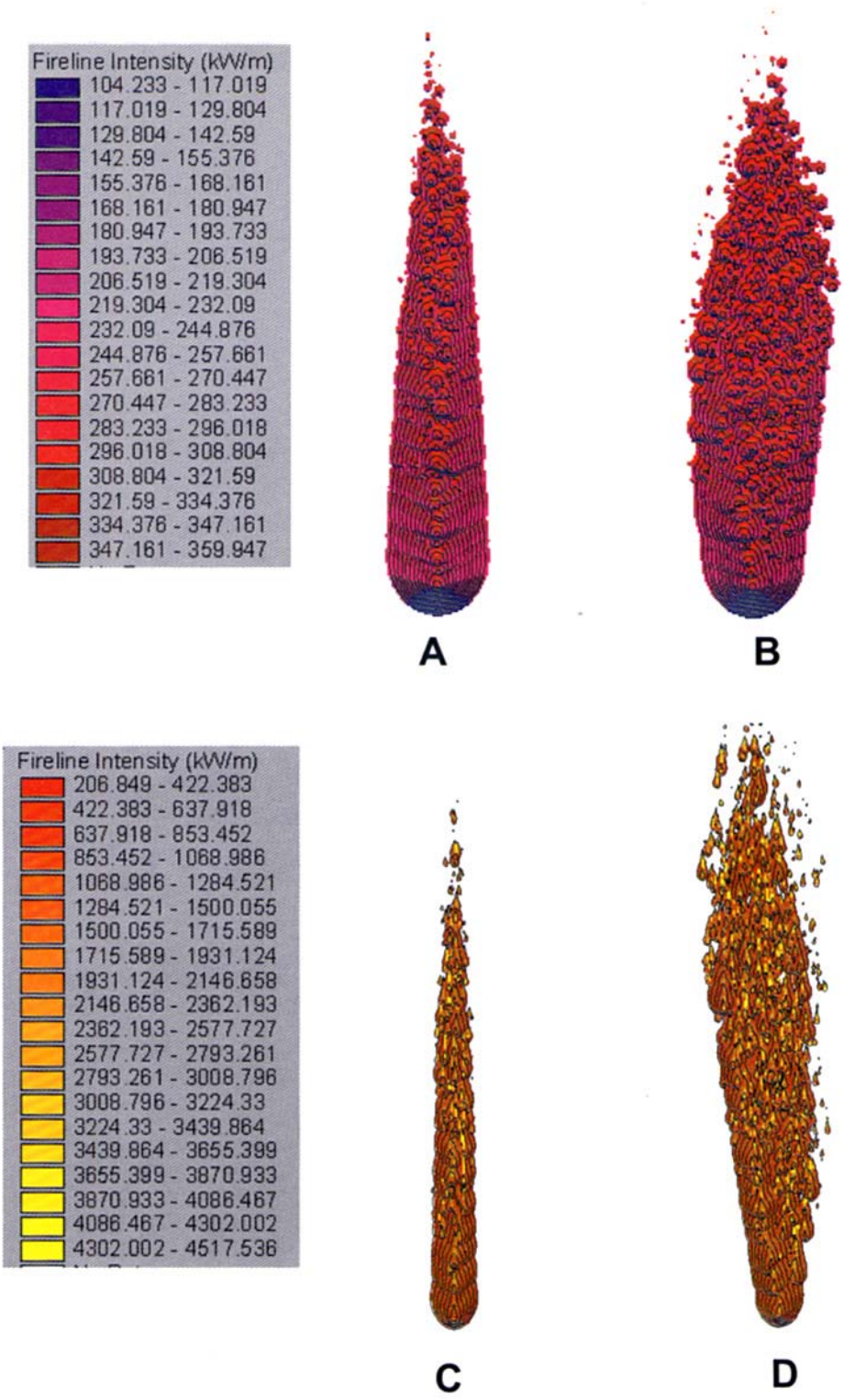

Color plate 10—Rippled patterns of intensity produced by spotting on flat terrain. **(A)** Passive crownfire with windspeed 8 m s^{-1}. **(B)** Passive crown fire with wind direction alternating 40° at regular intervals. **(C)** Active crownfire with 15 m s^{-1} windspeed. (**D)** Active crownfire with wind direction alternating 40° at regular intervals. Note that intensity range is much greater for active crown fire than passive crown fire. Surface fuel model 10, crown height = 15 m, canopy cover = 70 percent, crown bulk density = 0.25 kg m^{-3}, crown base height = 2.5 m.

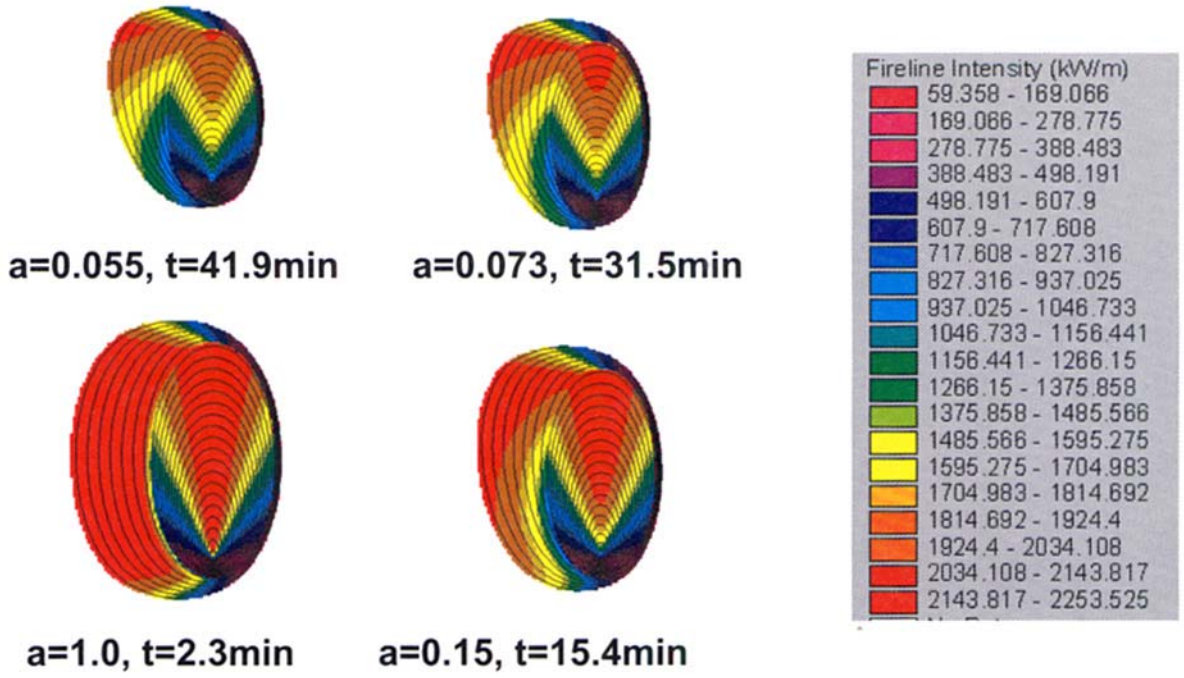

Color plate 11—Effects of fire acceleration rates on fire shapes on flat terrain with south wind for 20 minutes and east wind for 6 minutes. As acceleration rate a_a decreases (response time t increases), the slower spread rates of the rearward flanks prior to the wind shift take longer to respond to the new equilibrium spread rate after the wind shift.

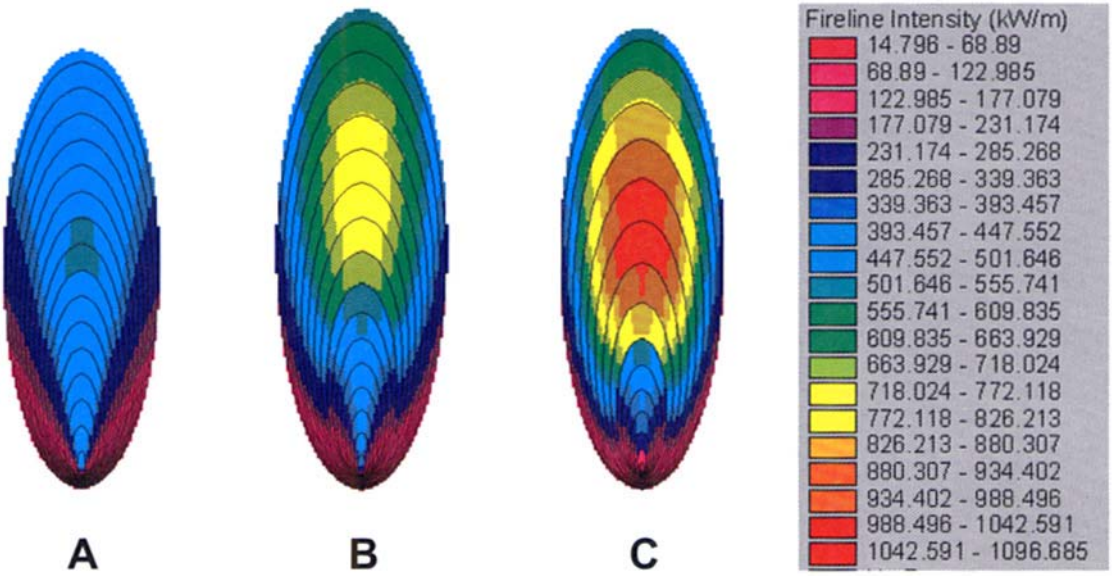

Color plate 12—Patterns of intensity change throughout the day depending on fuel moistures. Point source ignitions on flat terrain starting at 0600 and ending at 2200 hours, with **(A)** little change in temperature (70 to 71 °F) or humidity (41 to 40 percent), **(B)** moderate variation in temperature (40 to 80 °F) and humidity (60 to 30 percent), **(C)** high variation in temperature (40 to 90 °F) and humidity (90 to 20 percent).

Color plate 13—Tree-crown streets photographed after a crown fire in the New Jersey Pine Barrens are similar to crown fire simulations with alternating wind directions.

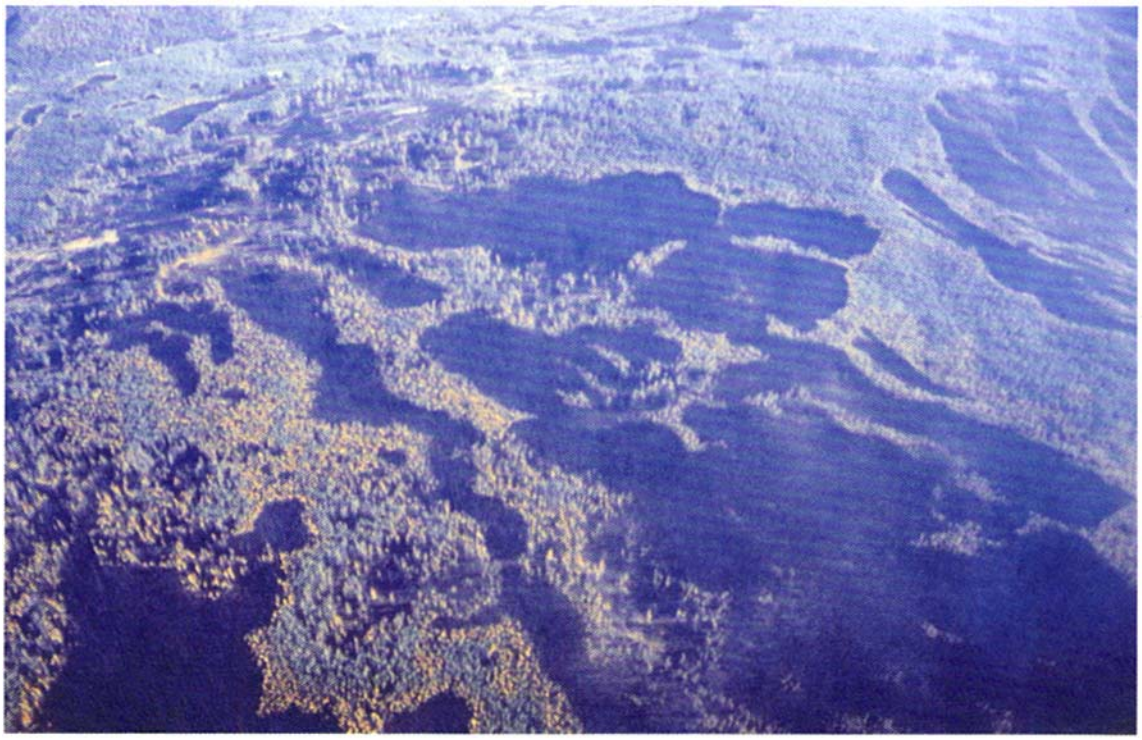

Color plate 14—Variable fire patterns in lodgepole pine forests photographed after the 1988 Yellowstone fires (photo by R. A. Hartford) are similar to the heterogeneity produced when spotting was simulated.

Finney, Mark A. Revised 2004. *FARSITE*: Fire Area Simulator—model development and evaluation. Res. Pap. RMRS-RP-4, Ogden,UT: U.S. Department of Agriculture, Forest Service, Rocky Mountain Research Station. 47 p.

A computer simulation model, *FARSITE,* includes existing fire behavior models for surface, crown, spotting, point-source fire acceleration, and fuel moisture. The model's components and assumptions are documented. Simulations were run for simple conditions that illustrate the effect of individual fire behavior models on two-dimensional fire growth.

Keywords: fire growth modeling, fire behavior models, fire simulation

You may order additional copies of this publication by sending your mailing information in label form through one of the following media. Please specify the publication title and number.

Telephone	(970) 498-1392
FAX	(970) 498-1396
E-mail	rschneider@fs.fed.us
Web site	http://www.fs.fed.us/rm
Mailing Address	Publications Distribution Rocky Mountain Research Station 240 West Prospect Road Fort Collins, CO 80526

Rocky Mountain Research Station
324 25th Street
Ogden, UT 84401

Federal Recycling Program Printed on Recycled Paper

The Rocky Mountain Research Station develops scientific information and technology to improve management, protection, and use of the forests and rangelands. Research is designed to meet the needs of National Forest managers, Federal and State agencies, public and private organizations, academic institutions, industry, and individuals.

Studies accelerate solutions to problems involving ecosystems, range, forests, water, recreation, fire, resource inventory, land reclamation, community sustainability, forest engineering technology, multiple use economics, wildlife and fish habitat, and forest insects and diseases. Studies are conducted cooperatively, and applications may be found worldwide.

Research Locations

Flagstaff, Arizona
Fort Collins, Colorado*
Boise, Idaho
Moscow, Idaho
Bozeman, Montana
Missoula, Montana
Lincoln, Nebraska
Reno, Nevada
Albuquerque, New Mexico
Rapid City, South Dakota
Logan, Utah
Ogden, Utah
Provo, Utah
Laramie, Wyoming

*Station Headquarters, 240 West Prospect Road, Fort Collins, CO 80526